



THE UNIVERSITY *of* EDINBURGH

Edinburgh Research Explorer

## Generating a link between a cell division and suicide gene provides a measure and solution for cell therapy safety

### Citation for published version:

Liang, Q, Monetti, C, Shutova, MV, Neely, EJ, Hacibekiroglu, S, Yang, H, Kim, C, Zhang, P, Li, C, Nagy, K, Mileikovsky, M, Gyongy, I, Sung, H-K & Nagy, A 2018, 'Generating a link between a cell division and suicide gene provides a measure and solution for cell therapy safety', *Nature*, vol. 563.

### Link:

[Link to publication record in Edinburgh Research Explorer](#)

### Document Version:

Peer reviewed version

### Published In:

Nature

### General rights

Copyright for the publications made accessible via the Edinburgh Research Explorer is retained by the author(s) and / or other copyright owners and it is a condition of accessing these publications that users recognise and abide by the legal requirements associated with these rights.

### Take down policy

The University of Edinburgh has made every reasonable effort to ensure that Edinburgh Research Explorer content complies with UK legislation. If you believe that the public display of this file breaches copyright please contact [openaccess@ed.ac.uk](mailto:openaccess@ed.ac.uk) providing details, and we will remove access to the work immediately and investigate your claim.



# Generating a link between a cell division and suicide gene provides a measure and solution for cell therapy safety

Qin Liang<sup>1,2,\*</sup>, Claudio Monetti<sup>1,\*</sup>, Maria V Shutova<sup>1</sup>, Eric J Neely<sup>1,2</sup>, Sabiha Hacibekiroglu<sup>1,2</sup>, Huijuan Yang<sup>1,3</sup>, Christopher Kim<sup>1,2</sup>, Puzheng Zhang<sup>1</sup>, Chengjin Li<sup>1</sup>, Kristina Nagy<sup>1,3</sup>, Maria Mileikovsky<sup>1</sup>, Istvan Gyongy<sup>4</sup>, Hoon-Ki Sung<sup>1,5</sup> and Andras Nagy<sup>1,2,6,7</sup>

<sup>1</sup> Lunenfeld-Tanenbaum Research Institute, Sinai Health System, Toronto, Canada

<sup>2</sup> Institute of Medical Science, University of Toronto, Toronto, Canada

<sup>3</sup> Department of Physiology, University of Toronto, Toronto, ON, Canada

<sup>4</sup> School of Mathematics and Maxwell Institute, The University of Edinburgh, Edinburgh, UK

<sup>5</sup> The Hospital for Sick Children Research Institute, Toronto, ON, Canada

<sup>6</sup> Australian Regenerative Medicine Institute, Monash University, Melbourne, VIC, Australia

<sup>7</sup> Department of Obstetrics & Gynaecology, University of Toronto, Toronto, ON, Canada

\* These authors contributed equally to this work.

Running Title: Defining cell therapy safety

Text word count Summary paragraph: 158

Text word count main text: 3245

Number of Figures: 4

Methods word count: 3327

Number of Extended Data Figures: 10

Number of Supplementary Tables: 3

Number of Supplementary Video: 1

Number of Supplementary Calculation: 1

*Keywords:* cell therapy, defining cell therapy safety, fail-safe cell system, fail-safe level, pluripotent stem cells, therapeutic cells, tumorigenicity, mutation rate, cell division essential locus, suicide gene, genome editing, human, mouse

*Corresponding author:* Andras Nagy, [nagy@lunenfeld.ca](mailto:nagy@lunenfeld.ca)

48 **The advent of human pluripotent cell lines holds enormous promise for the development of cell**  
49 **therapies to treat degenerative disease. Safety, however, is a crucial pre-condition for clinical**  
50 **application. Numerous groups have attempted to eliminate potentially harmful cells through the use**  
51 **of suicide genes<sup>1</sup>; however, none of these efforts quantitatively define safety. Here, we show a**  
52 **concept for the protection of a suicide transgene system from inactivation and its realisation with**  
53 **genome engineering strategies. The strategy behind our fail-safe (FS) design is to create a**  
54 **transcriptional link between the suicide gene herpes simplex virus-thymidine kinase (HSV-TK) and**  
55 **a cell division essential gene, Cyclin-Dependent Kinase 1 (*CDK1*). Furthermore, we add a**  
56 **quantitative measure to cell therapy safety as the function of the cell number needed for a therapy**  
57 **and the type of genome editing performed. Even with the highly conservative estimates described**  
58 **here, we anticipate that our solution and the quantification of safety will rapidly accelerate the entry**  
59 **of cell-based medicine to the clinic.**  
60

61 Most randomly integrated transgenes are not stably expressed in all cells. The transfected cell  
62 population will show variegated expression as a result of epigenetic and genetic modifications,  
63 developmental regulation, mutations, and/or complete loss of the transgene<sup>2-4</sup>. To alleviate these  
64 mechanisms, we generated a transcriptional link between a cell division essential locus (CDEL) and a  
65 drug-inducible suicide system (SU), resulting in a CDEL-SU allele (Fig. 1a). In this design, the expression  
66 of the CDEL and SU are tightly linked together, and if required, the dividing cells of a graft can be  
67 eliminated or arrested through treatment with the SU prodrug. With an SU placed in a CDEL essential for  
68 cell-life, the entire graft could be eliminated regardless of its proliferative status.

69 According to the engineering definition, fail-safe systems are designed to mitigate potential harm  
70 caused by a system failure. Using this terminology, a cell population is considered fail-safe if all of the  
71 cells within the population contain a functional SU. The fail-safe level (FSL) is defined as a number. It  
72 indicates that the odds of using a non-FS batch of cells for therapy is one out of this number (Fig. 1b),  
73 such as one out of a thousand (FSL=1,000) or one out of a million (FSL=1,000,000) batches. Here, we used  
74 various *in vitro* and *in vivo* experiments as well as mathematical modelling to define the FSL that needs to  
75 be satisfied for future cell therapies to be designated as safe.

76 To generate a list of CDEL candidates, we cross-referenced genes whose knock-out has an early  
77 embryonic lethal phenotype in mice (<http://www.informatics.jax.org/phenotypes.shtml>) with data from a  
78 genome-wide CRISPR/Cas9 mutagenesis screen for essential genes in human cancer cell lines<sup>5</sup>. We found  
79 167 genes with a high-fitness score ( $< -1.0$ )<sup>5</sup> that also have a known early-embryonic lethal phenotype  
80 (Supplementary Table 1). For this study, we chose *CDK1* as our prototype CDEL and an optimised mutant  
81 version of HSV-TK, TK.007<sup>6</sup> (TK from now on), as the SU prototype. Genetic studies have shown that  
82 *CDK1* is an essential kinase<sup>7</sup>. Its absence causes a block in the G2/M transition of the cell cycle, and other  
83 CDKs are not able to rescue its deficiency<sup>8,9</sup>. TK has been extensively used for cell ablation<sup>10</sup>, and its  
84 mechanism of action in the presence of its clinically-approved prodrug ganciclovir (GCV), is well  
85 characterised<sup>11</sup>. Importantly, *CDK1* and the linked TK are not expressed in non-dividing cells<sup>9</sup>, thus  
86 eliminating the potential immunogenicity of the viral TK protein<sup>12</sup> in quiescent donor cells.

87 To generate a transcriptional link between *CDK1* and TK (Fig. 1c), we used CRISPR/Cas9-assisted  
88 genome targeting to insert TK into the 3' untranslated region (3'UTR) of *CDK1* in mouse C2<sup>13</sup> (Extended  
89 Data Fig. 1a-d, 2a-c), human H1<sup>14</sup> (Extended Data Fig. 1e-i, 3a-f) and human CA1<sup>15</sup> (Extended Data Fig.  
90 4a-e) embryonic stem (ES) cells. Next, we determined the optimal GCV concentration for the  
91 heterozygous *CDK1*-TK mouse and human ES cells *in vitro* (Extended Data Fig. 2d, 3h), and then  
92 subsequently tested if we could control the growth of teratomas generated from these lines. Subcutaneous  
93 grafting of mouse ES cells into isogenic C57BL/6N recipients, and human ES cells into immunodeficient  
94 NOD scid gamma (NSG) recipients, resulted in teratoma formation with the expected efficiency (Extended  
95 Data Fig. 2e, 3g, 4d). When the volume of these tumours reached 500 mm<sup>3</sup> (considered as day 0), we

96 administered GCV daily by intraperitoneal injection for up to four weeks. Exposure to GCV rendered the  
97 C2 ES cell-derived teratomas dormant, without any sign of growth rebound following the treatment (Fig.  
98 1d, e and Extended Data Fig. 5a). The heterozygous H1 ES cell-derived teratomas in NSG mice responded  
99 similarly, albeit, in most of the cases, repeated and more extended GCV treatments were required to  
100 stabilise the teratoma size (Fig. 1f and Extended Data Fig. 5c). The observed decrease in teratoma size  
101 following GCV re-administration (Extended Data Fig. 5c) indicates that quiescent or slow-dividing cells  
102 within the teratoma began proliferating following drug withdrawal, and consequently, expressed TK and  
103 became sensitive to GCV. Furthermore, we found that the volume of the human teratomas frequently  
104 increased in the later phase of the experiments (Extended Data Fig. 5d); however, in agreement with  
105 previous reports<sup>16,17</sup>, this increase was the result of extensive cyst formation (Extended Data Fig. 5d) and  
106 not solid tissue growth. The induced long-term dormancy of the teratomas was encouraging but also  
107 unexpected as we predicted that such a large ES cell-derived tissue ( $\sim 10^9$  cells<sup>18</sup>) would contain hundreds  
108 of cells capable of escaping the SU through different types of mutations, such as silencing mechanisms  
109 and loss-of-heterozygosity (LOH). Within the well-encapsulated teratoma, however, it is likely that these  
110 assumed resistant cells (escapees) were eliminated by the known bystander killing effect of the TK/GCV  
111 system<sup>19</sup>.

112 To further investigate the capacity of the FS system to control cell proliferation, we also performed a  
113 breast cancer transplantation assay using heterozygous FS mammary epithelial tumour cells<sup>20</sup>. Upon  
114 transplantation in an isogenic setting, we observed that after a delayed period ( $\sim 100$  days) the  
115 heterozygous FS tumours became resistant to GCV and continued growing in the presence of the drug  
116 (Extended Data Fig. 6a,b).

117 To identify escapees appearing in the expansion of heterozygous FS ES cells, we designed an *in*  
118 *vitro* experiment to mitigate the bystander killing effect (Extended Data Fig. 7a,b) and subsequently  
119 characterised the resistance mechanism in the eight independent clonal escapee-lines we obtained from  
120 120 million cells. To determine if the escapee-generating mechanism was due to large genomic changes or  
121 *Cdk1*-TK locus-specific, we analysed the copy number (CN) of *Cdk1*, the TK transgene, and six additional  
122 endogenous genes all located on chromosome 10 (Fig. 1i, Extended Data Fig. 7d). Interestingly, this  
123 analysis revealed that only one escapee (E3 in Fig. 1i) contained the TK gene (Extended Data Fig. 7c).  
124 Further analyses did not detect mutations in the coding region of either *Cdk1* or TK (data not shown) but  
125 found the expression level of this allele was compromised and rendered the cells GCV resistant (Extended  
126 Data Fig. 7e). Another escapee, E5, was the result of a regional deletion involving the *Cdk1*-TK locus,  
127 and this led to at least an 18.5 Mbp hemizygous region in the wild type chromosome (predicted by CN=1  
128 in *Sim1*, *Rhobtb1*, *Cdk1* and *Ank3* genes (Fig. 1i, Extended Data Fig. 7d). Regarding the other six clones,  
129 the diploidy (CN=2) of all of the examined endogenous chromosome 10 genes and the lack (CN=0) of TK  
130 suggested that these six escapees were formed by diploid LOH (dLOH). This was likely due to mitotic  
131 recombination events or chromosomal non-disjunction which homozygosed the wild type *Cdk1* allele in  
132 a diploid form. In summary, our data indicate that dLOH is the dominant mechanism of losing the *Cdk1*-  
133 TK allele in heterozygous ES cells. This finding is consistent with a study of mouse *Aprt* heterozygous  
134 cells, where dLOH accounted for 78% of the observed loss of gene function events<sup>21</sup>.

135 To mitigate the generation of escapees by dLOH, we established both mouse and human ES cells  
136 homozygous for the *CDKI*-TK allele (Extended Data Fig. 2a-c, 3a-h, 4a-e). As expected, we were unable  
137 to identify any escapees when we repeated the above experiment (Extended Data Fig. 7b). It was not  
138 surprising that the homozygous ES cell-derived teratomas behaved similarly to the heterozygous  
139 teratomas; a brief GCV treatment was sufficient to render these tissues dormant (Fig. 1g,h, Extended Data  
140 Fig. 5b,e). As observed for the human heterozygous lines, cyst formation also occurred in the human  
141 homozygous teratomas (Extended Data Fig. 5e). Furthermore, we also generated homozygous FS  
142 mammary tumour cells and, following transplantation, observed that the size of these tumors could be  
143 reduced and their growth restrained through GCV administration (Extended Data Fig. 6c). The observed

144 growth rebound following GCV withdrawal was not surprising as slow-dividing or quiescent, tumour-  
145 prone MMTV-PyMT cells survive GCV administration and can start growing in the absence of the drug.  
146 Nevertheless, even in this non-clinical, extreme situation where a tumour cell line is used for cell  
147 transplantation, the homozygous FS system is still capable of managing and controlling tumour growth.  
148 Since we were unable to identify any escapees appearing in homozygous FS ES cell expansion, we used  
149 Monte Carlo (MC) simulation to estimate the odds of generating an escapee in this scenario. The model  
150 considers three different types of mutations which could affect the function of the CDEL-SU link (Fig.  
151 2a). Type 1 mutations (su1) render the SU non-functional while keeping the linked CDEL  
152 operational. Type 2 mutations (su2) eliminate both SU and CDEL functionality through epigenetic or  
153 genetic changes to the entire locus, including a hemizygous LOH-dependent mechanism. Type 3  
154 mutations remove a functional CDEL-SU allele by dLOH.

155 To estimate the probabilities of the type 1, 2 and 3 mutations ( $p_1$ ,  $p_2$  and  $p_3$ , respectively) per cell  
156 generation (Fig. 2a), we used our targeted human H1 *CDKI*-TK-mCherry/*CDKI*-TK-EGFP dichromatic  
157 cell line, as most mutations in either *CDKI*-TK allele result in monochromatic cells. We grew 21 parallel  
158 cultures from a single dichromatic cell to an average of  $5 \times 10^6$  cells per culture ( $> 22$  consecutive  
159 doublings) and determined the number of monochromatic cells in the culture using flow cytometry. Next,  
160 we applied Luria-Delbruck fluctuation analysis<sup>22,23</sup> to calculate the sum of the  $p_1+p_2+p_3$  probabilities in  
161 the two *CDKI*-TK alleles. We found that the mutation rate of losing mCherry was  $9.05 \times 10^{-6}$  per cell per  
162 division while the mutation rate of losing EGFP was similar at  $7.68 \times 10^{-6}$  per cell per division (Extended  
163 Data Fig. 8a-b).

164 To further validate the probabilities of these various mutations, we also analysed published studies  
165 that focused on these events. In mouse ES cells, the mutation rate ( $p_1+p_2+p_3$ ) of changing from a  
166 dichromatic to a monochromatic phenotype in the *Rosa26* locus (mouse Chr. 6) was  $1 \times 10^{-5}$  per cell, per  
167 division<sup>24</sup>. Similarly, another study calculated the mutation rate of gene function loss in the *Gdf9* locus  
168 (mouse Chr. 11) to be  $2.3 \times 10^{-5}$  events per cell per division<sup>25</sup>. Furthermore, the probability of the type 3  
169 mutation,  $p_3$  alone, has been calculated as  $1 \times 10^{-5}$ ,  $7.2 \times 10^{-6}$  and  $8.5 \times 10^{-6}$  in three different studies<sup>26-28</sup> by  
170 performing high G418 selection in mouse ES cells. The  $p_1+p_2$  mutation rate has also been estimated in  
171 the human *HPRT* locus on the X chromosome to be  $1.7-6 \times 10^{-7}$  by Luria-Delbruck fluctuation analysis<sup>29</sup>,  
172 and  $5 \times 10^{-6}$  through mutation frequency analysis in population datasets<sup>30</sup>.

173 Next, we performed MC simulation to establish the FSL of cell batches derived from different  
174 SU genotypes. Based on both published data and our own, we used the values  $p_1=p_2=10^{-6}$  and  $p_3=2 \times 10^{-5}$   
175 per cell per division; all of which are intentional overestimates. Consequently, our calculated FSLs  
176 represent underestimates, being equal or lower than the actual FSL.

177 *In silico*, we subsequently generated a sufficient number of cell batches that were expanded from  
178 a single cell with an intact SU system. In every doubling, the model permits allele transitions (Fig. 2b)  
179 which determine the transition graph (depicted in Fig. 2c); reflecting the genotype change that could occur  
180 during cell expansion. For the homozygous *CDKI*-TK/*CDKI*-TK simulation, we initiated the batch  
181 production from an SU/SU cell, while for the heterozygous *CDKI*-TK/*CDKI*<sup>wt</sup> simulation, the initiating  
182 cell was SU/su1. Lastly, for the compound heterozygous *CDKI*-TK/*CDKI*<sup>null</sup> simulation, the initiating  
183 cell was SU/su2, since the su1 is functionally equivalent to *CDKI*<sup>wt</sup>, while su2 is the same  
184 as a *CDKI*<sup>null</sup> allele (Fig. 2a).

185 A batch of cells is considered FS if it does not contain any escapees (Fig. 2d). The MC simulation  
186 determined the frequency of getting a non-FS batch of cells, which allowed us to calculate the FSL as the  
187 function of the cell number needed for a therapeutic cell batch. Fig. 2e shows these functions for the  
188 different initiating cell genotypes detailed above.

189 The number of cells required for a cell therapy is disease-specific and is estimated to range between  
190  $10^5$  (i.e. eye<sup>31,32</sup>) and  $10^{10}$  (i.e. heart<sup>33</sup>) cells. The genotype scenarios presented in Fig. 2e shows that a  
191 single TK insertion (*CDKI*-TK/*CDKI*<sup>wt</sup>, *CDKI*-TK/*CDKI*<sup>null</sup>) gives a low FSL for the cell numbers

192 required for therapy. Contrarily, a homozygous TK insertion into *CDKI* significantly increases the  
 193 FSL and brings the safety into a clinically relevant range for many future cell therapies. Diseases, such as  
 194 arthritis, diabetes or myocardial infarction, however, require a larger number of therapeutic cells ( $10^8$  to  
 195  $10^{10}$  donor cells). In this range, even the homozygous CDEL-SU provided FSL is insufficient ( $FSL < 10$ ).  
 196 For this disease category, we propose the homozygous modification of two different CDELS with suicide  
 197 genes. In this scenario, our MC simulation showed an enormous increase in FSL ( $FSL > 10^6$  for all  
 198 clinically relevant batch volumes, Fig. 2e).

199 We observed that the logarithm of FSL, as a function of the logarithm of the cell number, is a  
 200 convex function. It is very close to a linear function when the FSL is above 10 and the cell number is in  
 201 the clinically relevant range. Therefore, for an estimation of FSL, we applied linear regression to  
 202 these segments (Fig. 2e). Interestingly, the slope of the two linear regressions (Fig. 2e) is very close  
 203 to minus one (-0.99) and the y-intercepts of these lines were close to 9 and 16 for one and two CDEL  
 204 modifications, respectively. Using these approximates, the calculation of FSLs becomes  
 205 very simple, while remaining the desired underestimates (Fig. 2e):

206  
 207 For one CDEL:  $FSL = 10^9/cn$ , and for two CDELS:  $FSL = 10^{16}/cn$ , where  $cn$  is the cell number needed for  
 208 a therapeutic cell batch.

209  
 210 Concerning the production of cells for a specific therapy, some are lost during differentiation or  
 211 expansion. To account for this, the efficiency of cell production should be accurately estimated and the  
 212 cell number needed to generate a therapeutic batch should be corrected accordingly.

213 In future autologous cell therapies, the generation of multiple therapeutic batches might not be  
 214 necessary, and a single FS clone could be grown up to the number of cells required for therapy. On the  
 215 other hand, if allogeneic cells are desired or HLA haplobanks<sup>34</sup> of human pluripotent cell lines will be  
 216 operational, the generation of an off-the-shelf bank of cell batches would be advantageous. In this  
 217 scenario, it would be more practical and economical to produce a large pool of cells which, following  
 218 quality control (QC) analysis, could be aliquoted into therapeutic doses. Consequently, we calculated the  
 219 effect of aliquoting on FSL using both mathematical (Supplementary Calculation 1) and Monte-Carlo  
 220 modeling approaches. On the basis of our established *in silico* model (Fig. 2e), we simulated the process  
 221 of escapee accumulation until the final pool size reached  $2^{20}$  and  $2^{27}$  cells. In both of these scenarios, we  
 222 calculated escapee generation frequency distributions. Next, we randomly picked  $A$  aliquots from these  
 223 pools and calculated the mean number of “bad” aliquots (containing one or more escapee) in each case.  
 224 By dividing the overall number of aliquots  $A$  by the number of bad aliquots, we calculated the aliquot FSL  
 225 ( $FSL_{ap}$ ). The ratio between  $FSL_{ap}$  and the FSL of the cell population size  $2^{20}/A$  or  $2^{27}/A$  ( $FSL_a$ ), is shown  
 226 in Fig. 2f (red and orange lines, respectively). To confirm the results of this approach, we also calculated  
 227 the same ratio using only theoretical assessment, where the final equation is as follows (Fig. 2f, blue line):

228  
 229 
$$\frac{FSL_{ap}}{FSL_a} \approx \frac{1}{A(1 - \sum_{k=0}^{m-1} 2^{-k-1} (\frac{A-1}{A})^{2^k})}$$
 where  $A$  is the number of aliquots generated from  
 the pool of cells, and  $m$  is the integer part of the base  
 2 log of the aliquot size.

230  
 231 The decrease in FSL is largest when a small number of aliquots are used (Fig. 2f, blue line). Within  
 232 a practical range of aliquots (100-500), the FSL of the batches remains almost constant, with the  
 233 probability modeling slightly underestimating the FSL drop. Consequently, aliquoting results in an  
 234 approximately five-fold decrease in FSL using both approaches. The difference between aliquoting from  
 235 a  $2^{20}$  ( $\sim 10^6$ ) vs.  $2^{27}$  ( $\sim 10^9$ ) pool shows that the drop is moderately larger (Fig. 2f) when we generate  
 236 aliquots from a pool size that is close to the edge of the linear part on the original FSL graph (Fig. 2e).

237 Following the generation of every cell batch or pool, a quality control (QC) needs to be performed  
 238 to ensure that the originating cell was FS and consequently, the FSL calculation was correct. To

239 demonstrate the practicality of the QC process, we grew several batches of cells from a single,  
240 homozygous FS ES cell. At the early phase of expansion, we verified that both *CDKI*-TK alleles were  
241 expressed and intact in the batch-originating single cell using flow cytometry and through allele-specific  
242 PCR (Extended Data Fig. 9) and sequencing of the TK-coding region.

243 Both mouse and human ES cells with the homozygous modification of *CDKI* have normal ES cell  
244 morphology and self-renewing capacity in standard ES cell culture conditions (Fig. 3a,b). The cells  
245 differentiated into the three embryonic germ layers in teratomas (Fig. 3c,d). Furthermore, we  
246 generated chimeric mice from the *Cdk1*-TK heterozygous mouse ES cells, and after germline  
247 transmission, obtained viable heterozygous and then homozygous adult mice (Fig. 3e, Extended Data Fig.  
248 6a). Homozygous FS H1 human ES cells express pluripotency markers (Fig. 3f), and were successfully  
249 differentiated into retinal pigmented epithelial (RPE) cells<sup>35</sup> (Fig. 3g-i), adipocytes, osteocytes,  
250 chondrocytes (Fig. 3j), definitive endoderm (Fig. 3k), pharyngeal pouch endoderm<sup>36</sup> (Fig. 3l) and beating  
251 cardiomyocytes (Supplementary Video 1). Additionally, using *in vitro* neural differentiation, we  
252 demonstrated the selective killing of dividing cells by the FS system. As expected, following a brief GCV  
253 treatment, all mitotically active cells were eliminated while non-dividing cells were spared (Fig. 3m). This  
254 ability could represent a valuable safety measure prior to the transplantation of cells into a recipient.

255 Although we previously demonstrated the robustness of the FS system using a breast cancer  
256 transplantation assay, we also wanted to simulate a clinical cell transplantation scenario gone awry. To  
257 accomplish this, we subretinally injected a 3:1 mixture of human homozygous FS RPE cells and human  
258 homozygous FS ES cells (mCherry tagged) into the eyes of NSG mice. Among 4 injected eyes, we did  
259 not observe any cell growth from the ES cell component of the graft when GCV was administered 24  
260 hours post-injection for a period of 28 days, as a preventative measure (Fig. 4a-b, Extended Data Fig. 10a-  
261 c). In contrast, cell growth was detectable in 6 eyes that received an initial PBS treatment (Fig. 4c,  
262 Extended Data Fig. 10e-i). Importantly, even when GCV administration is delayed three weeks post-  
263 injection and cell growth has already been detected, the homozygous FS system efficiently stopped the  
264 growing ES cell-derived component of the graft; only non-dividing cells remained (Fig. 4c, Extended Data  
265 Fig. 10g-i). This experiment illustrates the ability of the FS system to selectively eliminate proliferating  
266 cells after cell transplantation. Furthermore, neither the initial nor the delayed GCV treatment affected the  
267 RPE graft or the integrity of the surrounding retinal tissue (Fig. 4b,c, Extended Data Fig. 10).

268 No therapy is without risk. Understanding and quantifying the risks associated with cell-based  
269 therapies is critical for the clinical advancement of regenerative medicine. Without a measurable safety  
270 system, it remains a challenging ambition to develop cell therapies that can treat degenerative diseases  
271 with an acceptable level of safety. We have developed a genome-editing strategy that allows a fundamental  
272 definition of safety, as well as a quantification of the safety level as a function of the cell number needed  
273 for any given cell therapy.

274 After transcriptionally linking a cell suicide element to a cell division essential locus, we  
275 mathematically defined and quantified the safety of our FS system. These calculated risks are highly  
276 conservative, and represent an underestimate of the actual safety level of the system, as they were  
277 performed using worst-case scenarios. This is necessary because the cells required for therapies (100  
278 thousand to 10 billion) will need to be grown *ex vivo*. These conditions entail serious risks compared to  
279 most *in vivo* settings, where functional immune cells constantly surveil and eliminate transformed cells<sup>37</sup>.  
280 Additionally, since the number of cells needed will necessitate a similar number of genome duplications,  
281 any possible mutation could arise. Some mutations, such as a dominant negative heterozygous P53 can  
282 lead to a growth advantage<sup>38</sup> that allows mutant cells to rapidly take over the entire population within a  
283 competitive culture environment. For these reasons, the safety of *in vitro*-generated therapeutic cells must  
284 be vigorously assessed.

285 The concept and genome-editing approach presented here not only addresses these concerns, but  
286 also allows one to define cell therapy safety in a quantitative way. We contend that the risks, as determined

287 through experimentation and calculation, are sufficiently low and that the FS system will become an  
288 indispensable component of prospective cell therapies. Moreover, our approach to assess and quantify the  
289 safety of cell-based therapies will be critical for informed decision making by the regulators, clinicians  
290 and patients who will advance the therapies that will transform modern medicine.

291

292

- 293 1. Li, W. & Xiang, A. P. Safeguarding clinical translation of pluripotent stem cells with suicide  
294 genes. *Organogenesis* **9**, 34–39 (2013).
- 295 2. Dobie, K. Variegated gene expression in mice. *Trends in Genetics* **13**, 127–130 (1997).
- 296 3. Yagyu, S., Hoyos, V., Del Bufalo, F. & Brenner, M. K. Multiple mechanisms determine the  
297 sensitivity of human-induced pluripotent stem cells to the inducible caspase-9 safety switch. *Mol*  
298 *Ther Methods Clin Dev* **3**, 16003–8 (2016).
- 299 4. Kotini, A. G., de Stanchina, E., Themeli, M., Sadelain, M. & Papapetrou, E. P. Escape Mutations,  
300 Ganciclovir Resistance, and Teratoma Formation in Human iPSCs Expressing an HSVtk Suicide  
301 Gene. *Mol Ther Nucleic Acids* **5**, e284 (2016).
- 302 5. Wang, T. *et al.* Identification and characterization of essential genes in the human genome.  
303 *Science* **350**, 1096–1101 (2015).
- 304 6. Preuß, E. *et al.* TK.007: A Novel, Codon-Optimized HSVtk(A168H) Mutant for Suicide Gene  
305 Therapy. *Human Gene Therapy* **21**, 929–941 (2010).
- 306 7. Diril, M. K. *et al.* Cyclin-dependent kinase 1 (Cdk1) is essential for cell division and suppression  
307 of DNA re-replication but not for liver regeneration. *Proceedings of the National Academy of*  
308 *Sciences* **109**, 3826–3831 (2012).
- 309 8. Santamaría, D. *et al.* Cdk1 is sufficient to drive the mammalian cell cycle. *Nature* **448**, 811–815  
310 (2007).
- 311 9. Satyanarayana, A. *et al.* Genetic substitution of Cdk1 by Cdk2 leads to embryonic lethality and  
312 loss of meiotic function of Cdk2. *Development* **135**, 3389–3400 (2008).
- 313 10. Fillat, C., Carrio, M., Cascante, A. & Sangro, B. Suicide Gene Therapy Mediated by the Herpes  
314 Simplex Virus Thymidine Kinase Gene / Ganciclovir System: Fifteen Years of Application.  
315 *Current gene therapy* **3**, 13–26 (2003).
- 316 11. Tomacic, M. T., Thust, R. & Kaina, B. Ganciclovir-induced apoptosis in HSV-1 thymidine kinase  
317 expressing cells: critical role of DNA breaks, Bcl-2 decline and caspase-9 activation. *Oncogene*  
318 **21**, 2141–2153 (2002).
- 319 12. Berger, C., Flowers, M. E., Warren, E. H. & Riddell, S. R. Analysis of transgene-specific immune  
320 responses that limit the in vivo persistence of adoptively transferred HSV-TK-modified donor T  
321 cells after allogeneic hematopoietic cell transplantation. *Blood* **107**, 2294–2302 (2006).
- 322 13. Gertsenstein, M. *et al.* Efficient generation of germ line transmitting chimeras from C57BL/6N  
323 ES cells by aggregation with outbred host embryos. *PLoS ONE* **5**, e11260–e11260 (2010).
- 324 14. Thomson, J. A. *et al.* Embryonic stem cell lines derived from human blastocysts. *Science* **282**,  
325 1145–1147 (1998).
- 326 15. Adewumi, O. *et al.* Characterization of human embryonic stem cell lines by the International  
327 Stem Cell Initiative. *Nature Biotechnology* **25**, 803–816 (2007).
- 328 16. Damjanov, I. & Andrews, P. W. Teratomas produced from human pluripotent stem cells  
329 xenografted into immunodeficient mice - a histopathology atlas. *Int. J. Dev. Biol.* **60**, 337–419  
330 (2016).
- 331 17. Wu, S. M. & Hochedlinger, K. Harnessing the potential of induced pluripotent stem cells for  
332 regenerative medicine. *Nat. Cell Biol.* **13**, 497–505 (2011).
- 333 18. Bianconi, E. *et al.* An estimation of the number of cells in the human body. *Ann. Hum. Biol.* **40**,  
334 463–471 (2013).



- 335 19. Mesnil, M. & Yamasaki, H. Bystander effect in herpes simplex virus-thymidine  
336 kinase/ganciclovir cancer gene therapy: role of gap-junctional intercellular communication.  
337 *Cancer Research* **60**, 3989–3999 (2000).
- 338 20. Guy, C. T., Cardiff, R. D. & Muller, W. J. Induction of mammary tumors by expression of  
339 polyomavirus middle T oncogene: a transgenic mouse model for metastatic disease. *Molecular*  
340 *and Cellular Biology* **12**, 954–961 (1992).
- 341 21. Cervantes, R. B., Stringer, J. R., Shao, C., Tischfield, J. A. & Stambrook, P. J. Embryonic stem  
342 cells and somatic cells differ in mutation frequency and type. *Proceedings of the National*  
343 *Academy of Sciences* **99**, 3586–3590 (2002).
- 344 22. Luria, S. E. & Delbrück, M. Mutations of Bacteria from Virus Sensitivity to Virus Resistance.  
345 *Genetics* **28**, 491–511 (1943).
- 346 23. Capizzi, R. L. & Jameson, J. W. A table for the estimation of the spontaneous mutation rate of  
347 cells in culture. *Mutat. Res.* **17**, 147–148 (1973).
- 348 24. Larson, J. S., Yin, M., Fischer, J. M., Stringer, S. L. & Stringer, J. R. Expression and loss of  
349 alleles in cultured mouse embryonic fibroblasts and stem cells carrying allelic fluorescent protein  
350 genes. *BMC Mol Biol* **7**, 36 (2006).
- 351 25. Luo, G. *et al.* Cancer predisposition caused by elevated mitotic recombination in Bloom mice.  
352 *Nat Genet* **26**, 424–429 (2000).
- 353 26. Mortensen, R. M., Conner, D. A., Chao, S., Geisterfer-Lowrance, A. A. & Seidman, J. G.  
354 Production of homozygous mutant ES cells with a single targeting construct. *Molecular and*  
355 *Cellular Biology* **12**, 2391–2395 (1992).
- 356 27. Koike, H. *et al.* Efficient biallelic mutagenesis with Cre/loxP-mediated inter-chromosomal  
357 recombination. *EMBO Rep.* **3**, 433–437 (2002).
- 358 28. Yusa, K., Horie, K., Kondoh, G., Kouno, M. & Maeda, Y. Genome-wide phenotype analysis in  
359 ES cells by regulated disruption of Bloom's syndrome gene. *Nature* (2004).
- 360 29. Monnat, R. J. Molecular analysis of spontaneous hypoxanthine phosphoribosyltransferase  
361 mutations in thioguanine-resistant HL-60 human leukemia cells. *Cancer Research* (1989).
- 362 30. Green, M. H. L., O'Neill, J. P. & Cole, J. Suggestions concerning the relationship between mutant  
363 frequency and mutation rate at the hprt locus in human peripheral T-lymphocytes. *Mutation*  
364 *Research/Environmental Mutagenesis and Related Subjects* **334**, 323–339 (1995).
- 365 31. Schwartz, S. D. *et al.* Human embryonic stem cell-derived retinal pigment epithelium in patients  
366 with age-related macular degeneration and Stargardt's macular dystrophy: follow-up of two open-  
367 label phase 1/2 studies. *The Lancet* **385**, 509–516 (2015).
- 368 32. Mandai, M. *et al.* Autologous Induced Stem-Cell-Derived Retinal Cells for Macular  
369 Degeneration. *N. Engl. J. Med.* **376**, 1038–1046 (2017).
- 370 33. Chong, J. J. H. *et al.* Human embryonic-stem-cell-derived cardiomyocytes regenerate non-human  
371 primate hearts. *Nature* **510**, 273–277 (2014).
- 372 34. Barry, J., Hyllner, J., Stacey, G., Taylor, C. J. & Turner, M. Setting Up a Haplobank: Issues and  
373 Solutions. *Curr Stem Cell Rep* **1**, 110–117 (2015).
- 374 35. Klimanskaya, I. *et al.* Derivation and Comparative Assessment of Retinal Pigment Epithelium  
375 from Human Embryonic Stem Cells Using Transcriptomics.  
376 <http://www.liebertpub.com.myaccess.library.utoronto.ca/clo> **6**, 217–245 (2004).
- 377 36. Sun, X. *et al.* Directed Differentiation of Human Embryonic Stem Cells into Thymic Epithelial  
378 Progenitor-like Cells Reconstitutes the Thymic Microenvironment In Vivo. *Stem Cell* **13**, 230–  
379 236 (2013).
- 380 37. Dunn, G. P., Bruce, A. T., Ikeda, H., Old, L. J. & Schreiber, R. D. Cancer immunoediting: from  
381 immunosurveillance to tumor escape. *Nature Immunology* **3**, 991–998 (2002).
- 382 38. Merkle, F. T. *et al.* Human pluripotent stem cells recurrently acquire and expand dominant

383 negative P53 mutations. *Nature* **545**, 229–233 (2017).

384  
385  
386 Supplementary Information is linked to the online version of the paper at [www.nature.com/nature](http://www.nature.com/nature).

387  
388 **Acknowledgements** We thank the TCP Transgenic Core and Marina Gertsenstein for mouse line  
389 derivation, Annie Bang for flow cytometry, the TCP Pathology Core and Ken Harpal for histology  
390 analysis, Malgosia Kownacka for providing MEFs, Molly S. Shoichet for HAMC and Nikolaos  
391 Mitrousis for Q-PCR primers. We are also grateful to Sergey Nurk for advice on Monte Carlo  
392 simulation, to Iacovos P. Michael, Peter D. Tonge, Balasz V. Varga, Chen He and Rana El-Rass for  
393 experimental advice and Jeffrey S. Harding, and Kathryn C. Davidson for their proof-reading of the  
394 manuscript, to JSH for artwork. This work was supported by the CIHR foundation scheme, Canadian  
395 Research Chair and Medicine by Design (University of Toronto) to AN.

396  
397 **Author Contributions** Q.L. and C.M. designed and conducted most of the experiments, analysed the  
398 data, and wrote the manuscript. M.V.S. conducted the Monte Carlo simulations and analysed the  
399 data. I.G. performed the mathematical modelling. E.J.N. conducted experiments and wrote the  
400 manuscript. S.H. performed the eye experiment and analysed the data. H.Y., C.K., P.Z., C.L., K.N.,  
401 M.M., H.S. conducted experiments. A.N. conceived and supervised the study, designed experiments,  
402 analysed the data and wrote the manuscript.

403  
404 **Author Information** Reprints and permissions information is available at [www.nature.com/reprints](http://www.nature.com/reprints).  
405 A.N., C.M. and Q.L. are inventors on a patent application covering the FS technology  
406 (PCT/CA2016/050256). A.N. is the co-founder and shareholder of panCELLa Inc. C.M. is a senior  
407 scientist at panCELLa Inc. The other authors declare no competing interests. Correspondence and  
408 requests for materials should be addressed to A.N. ([nagy@lunenfeld.ca](mailto:nagy@lunenfeld.ca)).  
409

## 410 **Methods**

411 **Generation of targeting vectors.** Targeting vectors were generated by DNA synthesis, molecular  
412 cloning, recombineering and the NEBuilder HiFi DNA Assembly Cloning Kit (New England Biolabs).

413 **Generation of CRISPR/Cas9 vectors.** pX330-U6-Chimeric\_BB-CBh-hSpCas9 was a gift from Feng  
414 Zhang (Addgene plasmid # 42230)<sup>39</sup>. Guide sequences for CRISPR/Cas9 were analyzed using the  
415 online CRISPR design tool (<http://crispr.mit.edu>). Guide sequence for mouse *Cdk1* targeting:  
416 TAAGAAGATGTAGCCCTC. Guide sequence for human *CDK1* targeting:  
417 CTATCTGTTGACATAACATA.

418 **Mouse ES cell culture.** C57BL/6N C2 ES cells were grown at 37°C in 95% air 5% CO<sub>2</sub> on MEFs  
419 obtained from TgN(DR4)1Jae/J mice (<http://jaxmice.jax.org/strain/003208.html>) at all times except for  
420 one passage on gelatinized tissue culture plates prior to aggregation<sup>40</sup>. Two types of media were used:  
421 1). FBS-DMEM ES cell medium for gene targeting consisted of high glucose DMEM supplemented  
422 with 15% FBS (previously shown to support germline chimera generation), 2 mM GlutaMAX, 1 mM  
423 Na Pyruvate, 0.1 mM non-essential amino acids (NEAA), 50 U/ml penicillin and streptomycin (all  
424 Thermo Fisher Scientific), 0.1 mM 2-mercaptoethanol (Sigma) and 1000 U/ml LIF prepared with LIF  
425 producing plasmid.<sup>41</sup> 2). KOSR+2i medium was used for 2-4 passages prior to the generation of ES  
426 cell chimeras<sup>13</sup>. KOSR+2a consisted of high glucose DMEM medium supplemented with 15%

427 KnockOut Serum Replacement (KOSR) (Thermo Fisher Scientific), 1 mM Na Pyruvate, 0.1 mM  
428 NEAA, 0.1 mM 2-mercaptoethanol, 2 mM GlutaMAX, 50 U/ml penicillin/streptomycin, 500 U/ml  
429 LIF, 5 mg/ml Insulin (Thermo Fisher Scientific), 1  $\mu$ M of the mitogen-activated protein kinase inhibitor  
430 PD0325901 (StemGent) and 3  $\mu$ M of the glycogen synthase kinase-3 inhibitor CHIR99021  
431 (StemGent). Cells were fed daily and passaged when they reached a confluency of 70-80%. 0.05%  
432 Trypsin-EDTA (Thermo Fisher Scientific) was used for the passage of cells grown in FBS-DMEM and  
433 Accutase (STEMCELL Technologies) was used for cells grown in KOSR+2i medium.

434 **Mouse ES cell targeting.** 50,000 mouse C57BL/6N C2 ES cells were transfected with 2  $\mu$ g DNA  
435 (Mouse Target Vector 1 or 2: 1.5  $\mu$ g, CRISPR vector: 0.5  $\mu$ g) by JetPrime transfection (Polyplus). The  
436 cells were selected for G418-resistance (160  $\mu$ g/ml) starting 48h after transfection. Resistant clones  
437 were picked independently and replicated in 96-well plates for freezing and genotyping with PCRs.  
438 PCR-positive clones were expanded, frozen to multiple vials, and genotyped by Southern blotting.

439 **Selection cassette excision in mouse ES cells.** Correctly targeted ES cell clones were transfected with  
440 episomal-hyPBase (for Mouse Target Vector I) or pCAGGs-NLS-Cre-IRES-puromycin (for Mouse  
441 Target Vector II). 2-3 days following transfection, cells were trypsinized and plated clonally (1,000 -  
442 2,000 cells per 10 cm plate). mCherry-positive clones were picked and transferred to 96-well plates  
443 independently and genotyped by PCR and Southern blotting to confirm the excision event. The  
444 junctions of the removal region were PCR-amplified, sequenced, and confirmed to be intact and  
445 without any frameshift mutations. GCV (Sigma) to test for TK activity was used at a final concentration  
446 of 1  $\mu$ M.

447 **Human ES cell culture.** Human CA1 and H1 ES cells were cultured on Geltrex (Thermo Fisher  
448 Scientific) using mTeSR1 media (STEMCELL Technologies) containing 50 U/ml  
449 penicillin/streptomycin (Thermo Fisher Scientific). Cells were passaged using Tryple Express  
450 (Thermo Fisher Scientific) and were subsequently plated in mTeSR media containing 10  $\mu$ M ROCK  
451 inhibitor (Selleckchem) for 24 hours.

452 **Human ES cell targeting.** For Human Targeting Vectors I & II, 6 million human ES cells were  
453 electroporated using Neon Transfection System (Thermo Fisher Scientific) with protocol 14 (pulse  
454 voltage: 1200 mV, pulse width: 20 ms, pulse number: 2) with 24  $\mu$ g DNA (Target Vector: 18  $\mu$ g,  
455 CRISPR vector: 6  $\mu$ g). After transfection, cells were plated on four 10 cm plates. G418 selection at 30  
456  $\mu$ g/ml or puromycin selection at 0.75  $\mu$ g/ml was initiated 48h after transfection. Independent colonies  
457 were picked to 96-well plates and each plate was duplicated for further growth and genotyping with  
458 PCR. PCR-positive clones were expanded, frozen to multiple vials, and genotyped with Southern  
459 blotting. For Human Target Vector III targeting, 10 million human ES cells were electroporated using  
460 Neon protocol 14 with 40  $\mu$ g DNA (Human Target Vector III: 30  $\mu$ g, CRISPR vector: 10  $\mu$ g), and  
461 plated in four 10 cm plates. 3-4 days after transfection, cells that were double-positive for mCherry and  
462 eGFP were sorted into one well of a 96-well plate. After recovery from FACS, cells were dissociated  
463 and plated clonally (1,000 - 2,000 cells per 10 cm plate). Next, clones were picked independently,  
464 replicated, and transferred to 96-well plates for freezing and genotyping with PCR. PCR-positive  
465 clones were expanded, frozen to multiple vials, and genotyped by Southern blotting.

466 **Selection cassette excision in human ES cells.** 1 million correctly targeted ES cell clones were  
467 electroporated with 2  $\mu$ g episomal-hyPBase-IRES-puro (for Human Target Vector I) or 2  $\mu$ g episomal-  
468 Cre-IRES-puro (for Human Target Vector II) using Neon protocol 14. Once the cells were confluent  
469 in 6-well plates, mCherry-positive cells were sorted to one well of a 96-well plate by FACS. After  
470 recovery, cells were dissociated and plated clonally (1,000 - 2,000 cells per 10 cm plate). Clones were

471 picked and transferred to 96-well plates independently and genotyped by PCR and Southern blotting  
472 to confirm the excision event. The junctions of the removal region were PCR-amplified, sequenced  
473 and confirmed to be intact and without frameshift mutations.

474 **PCR genotyping.** 2X Taq PCR master mix (Biomart) was used for all PCR reactions. Genomic DNA  
475 from human cell pellets was extracted using the DNeasy Blood & Tissue Kit (Qiagen). The primer  
476 pairs and conditions used for each reaction are listed in Supplementary Table 2.

477 **Southern blotting.** 10 µg of genomic DNA was extracted from PCR-positive clones, digested with  
478 ScaI-HF overnight, resolved by 0.6 - 0.7% gel electrophoresis, and transferred to Hybond N+ (GE  
479 Healthcare). The following probes were labelled with <sup>32</sup>P and used to hybridize with the membrane  
480 (~25 ng probe per ml hybridization solution). Human *CDK1* genomic probe: PCR amplified with  
481 primers h*CDK1*-Probe6-F + h*CDK1*-Probe6-R. Mouse *Cdk1* genomic probe: PCR amplified with  
482 primers 647302FWD + 647302REV. mCherry probe: the entire length of mCherry. eGFP probe: the  
483 entire length of eGFP. TK-mCherry probe: cut from h*CDK1*-PB-neo-TK-mCherry with  
484 Bsu36I+SgrAI: 1092 bp, gel-purified.

485 **Mice.** The CD-1 (ICR) (Charles River) outbred albino stock was used as embryo donors for aggregation  
486 with ES cells and as pseudopregnant recipients. C57BL/6NCrI (Charles River) was used as the host for  
487 teratoma assays with mouse C2 ES cells. C57BL/6NCrI or B6N-Tyr\_c N4/CrI#493 (Charles River)  
488 was used as the host for mammary fat pad transplantation of mammary epithelial cells. NOD scid  
489 gamma /J#5557 (Jackson Laboratories) was used as the host for teratoma assays with human H1 or  
490 CA1 ES cells. FVB/N-Tg(MMTV-PyVT)634Mul/J was a gift from Dr. William Muller's lab<sup>20</sup>, and the  
491 backcross to B6J background was done by Dr. Anthony Pawson's lab. Animals were maintained on a  
492 12 h light/dark cycle and provided with food and water *ad libitum* in individually ventilated units  
493 (Techniplast) in the specific-pathogen free facility at The Centre for Phenogenomics (TCP). All  
494 procedures involving animals were performed in compliance with the Animals for Research Act of  
495 Ontario and the Guidelines of the Canadian Council on Animal Care.

496 **Generation of chimeras and mouse lines.** Morula aggregations were performed as previously  
497 described<sup>40</sup>. Chimeras were identified at birth by the presence of black eyes and later by coat  
498 pigmentation. Male chimeras with more than 50% ES cell contribution to coat colour were bred with  
499 CD-1 females to identify germline transmitter. The transmitter was then bred with C57BL/6NCrI  
500 females and pups were confirmed by genotyping to obtain *Cdk1*-TK/*Cdk1* mice. *Cdk1*-TK/*Cdk1*  
501 MMTV-PyMT males were generated by breeding MMTV-PyMT (B6) males and *Cdk1*-TK/*Cdk1*  
502 females. *Cdk1*-TK/*Cdk1*; MMTV-PyMT and *Cdk1*-TK/*Cdk1*-TK; MMTV-PyMT female mice were  
503 generated by breeding *Cdk1*-TK/*Cdk1*; MMTV-PyMT males and *Cdk1*-TK/*Cdk1* females.

504 **Teratoma assay.** Matrigel Matrix High Concentration (Corning) was diluted 1:3 with cold DMEM  
505 media on ice. 1-5 million mouse ES cells or 5-10 million human ES cells were suspended in 100 µl of  
506 Matrigel-DMEM and injected subcutaneously into one or both dorsal flanks of C57BL/6NCrI mice  
507 (for mouse C2 ES cells) and NOD scid gamma /J#5557 mice (for human H1 and CA1 ES cells).  
508 Teratomas formed 2-4 weeks after injection. Teratoma size was measured using calipers and volume  
509 was calculated using the formula  $V = (L \times W \times H) \pi / 6$ . GCV /PBS treatment was performed through daily  
510 intraperitoneal injections (50 mg/kg) with varying treatment durations. At the end of treatment, mice  
511 were sacrificed and tumors were dissected and fixed in 4% paraformaldehyde for histological analysis.

512 **Breast cancer transplantation assay.** *Cdk1-TK/Cdk1*; MMTV-PyMT and *Cdk1-TK/Cdk1-TK*;  
513 MMTV-PyMT female mice developed mammary gland tumours between 3-6 months old. Mammary  
514 epithelial tumorigenic cells were isolated from developed tumours through digestion in 10×  
515 collagenase/hyaluronidase (STEMCELL Technologies), and dilution to 1x with media consisting of  
516 DMEM/F12 (Thermo Fisher Scientific) + 10% FBS + 50 U/ml penicillin/streptomycin for an hour in  
517 37 degree. The digested cells were washed and pelleted with DMEM/F12 + 10% FBS 4 times, and  
518 plated in CnT-PRIME epithelium culture media (CELLnTEC Advanced Cell Systems AG) on plates  
519 coated with 0.1% gelatin (Sigma). Without passaging, primary mammary epithelial cells were  
520 dissociated and re-suspended in PBS at 10,000 cells per µl, and 50 µl (500,000 cells) was transplanted  
521 to each mouse by intraductal injection after making a small abdominal skin incision as previously  
522 described<sup>42</sup>. Tumour measurement and PBS/GCV treatment were the same as described in the teratoma  
523 assay.

524 **Differentiation of human ES cells into retinal pigmented epithelial (RPE) cells.** RPE differentiation  
525 was performed as previously described<sup>35</sup> with minor changes. Human ES cells were plated on Geltrex-  
526 coated 6-well plates and cultured in feeder-free conditions with mTeSR medium until confluency was  
527 reached and the colonies lost their tight borders (7-10 days). Next, the media was replaced with  
528 differentiation media (basal media with 13% KOSR) and changed every 2-3 days. The basal media  
529 consisted of KO-DMEM supplemented with 50 U/ml penicillin/streptomycin mix, 1 mM Na Pyruvate,  
530 0.1 mM NEAA, 2 mM of GlutaMAX and 0.1 mM 2-mercaptoethanol. Initial pigmentation was  
531 observed approximately 3 weeks after the switch to differentiation media. Clusters of RPE cells were  
532 manually picked and transferred to a Geltrex-coated 24-well plate (3 clusters/well) when they were  
533 large enough (~1mm in diameter) for enrichment and the media was changed to RPE media, consisting  
534 of basal media with 5% FBS, 7% KSR and 10 ng/ml bFGF (Peprotech).

535 **Differentiation of human ES cells into definitive endoderm.** Definitive endoderm differentiation  
536 was performed using the STEMdiff Trilineage Differentiation Kit (StemCell Technologies), and  
537 characterized by immunostaining for SOX17 and FOXA2 (Supplementary Table 3).

538 **Differentiation of human ES cells into pharyngeal pouch endoderm (PPE).** PPE differentiation  
539 was performed as previously described<sup>36</sup> with the only modification being that the induction from ES  
540 cells to definitive endoderm is one day shorter than reported.

541 **Differentiation of human ES cells into mesenchymal stem cells (MSCs) and subsequent**  
542 **adipogenic, osteogenic and chondrogenic differentiation.** ES cells were cultured in mTeSR medium  
543 for 2 days. Next, cells were induced into early mesoderm progenitor cells with STEMdiffMesenchymal  
544 Induction Medium (STEMCELL Technologies) for 4 days and then were maintained with MesenCult-  
545 ACF Medium (STEMCELL Technologies). Cells were continually passaged onto 6-well plates pre-  
546 coated with MesenCult-ACF Attachment Substrate (STEMCELL Technologies) to derive early  
547 mesenchymal progenitor cells. At day 21, the MSCs showed a fibroblast-like morphology and the  
548 culture medium was changed every 3 days. For adipogenic differentiation, MSCs at a density of 20,000  
549 cells/well were plated with MesenCult-ACF Attachment Substrate and cultured with MesenCult-ACF  
550 Medium for 2 days. Adipogenesis was induced using the StemPro Adipogenesis Differentiation Kit  
551 (Thermo Fisher Scientific). After 21 days, lipid droplets were visualized using Oil Red O (Sigma). For  
552 osteogenic differentiation, ES-derived MSCs at the density of 50,000 cells/well were plated with  
553 MesenCult-ACF Attachment Substrate and cultured with MesenCult-ACF Medium for 2 days.  
554 Osteogenesis was induced using the StemPro Osteogenesis Differentiation Kit (Thermo Fisher  
555 Scientific). After 21 days, calcium deposition was visualized using Alizarin Red (Sigma). For induction  
556 of chondrogenic differentiation, ES-derived MSCs were centrifuged in 15 ml conical tubes at 500g for

557 5 mins to create cell pellets with 5,000,000 cells per pellet. Chondrogenesis was induced using the  
558 StemPro Chondrogenesis Differentiation Kit (Thermo Fisher Scientific). After 21 days, cartilage was  
559 visualized using Alcian Blue (Sigma). Differentiation media was changed every 3 days.

560 **Differentiation of human ES cells into beating cardiomyocytes.** Cardiomyocyte differentiation was  
561 performed using STEMdiff Cardiomyocyte Differentiation Kit (STEMCELL Technologies).

562 **Differentiation of human ES cells into neuronal progenitors and neurons.** To differentiate human  
563 ES cells into neuronal progenitors, human ES cells were plated at 50-100,000 cells per cm<sup>2</sup> in 1:1  
564 DMEM/F12 : Neurobasal (Thermo Fisher Scientific), 0.5x N2 supplement (home-made, 1.92 mg/ml  
565 putrescine, 2.376 µg/mL progesterone, 3.6 µM Selenium, 10 mg/mL Apo-transferrin, 0.75% BSA, 20  
566 g/ml insulin), 0.5x B27 supplement with Vitamin A (Thermo Fisher Scientific), 2 mM Glutamax, 0.1  
567 mM Beta-mercaptoethanol, 50 U/ml penicillin/streptomycin, 10 µM SB431542 (Selleckchem), 100  
568 nM LDN193189 (Selleckchem) (+10 µM ROCK inhibitor overnight only, then removed). Cells were  
569 maintained in this condition for 8 days and media was changed every other day. Next, neuronal  
570 progenitors were dissociated with Accutase and plated at a density of 5x10<sup>4</sup> cells per cm<sup>2</sup> on laminin  
571 (Sigma, 1 µl for 1cm<sup>2</sup>, diluted in 250 µl PBS without Ca and Mg) in fast neuron differentiation media,  
572 1:1 DMEM-F12: Neurobasal, 1x B27 supplement with Vitamin A, 5 µM DAPT (Selleckchem), 2 mM  
573 Glutamax, 0.1 mM Beta-mercaptoethanol, 50 U/ml penicillin/streptomycin. Media were changed every  
574 three days. 10 µM GCV was added 6 days after neuron differentiation and kept for 6 days. 10 µM BrdU  
575 (Sigma) was added after 5 days of GCV treatment and the cultures were fixed after 6 days of GCV  
576 treatment and were immunostained for BrdU and beta-TubulinIII (Supplementary Table 3).

577 **Flow cytometry analysis and fluorescence-activated cell sorting (FACS).** Flow cytometry and  
578 FACS were both performed and analyzed by the Lunenfeld-Tanenbaum Research Institute flow  
579 cytometry facility. FACS was performed using the ASTRIOS EQ cell sorter. Flow cytometry was  
580 performed using the GALLIOS flow cytometer and evaluated using Kaluza Analysis Software  
581 (Beckman Coulter). Samples were gated for live single cells using forward scatter, side scatter and  
582 DAPI staining. Wild-type and single-color samples of the same cell type as the experimental samples  
583 were used for negative controls and compensation calculations. Human ES cell samples were single-  
584 cell sorted using StemFlex Medium (Thermo Fisher Scientific) plus 10 µM ROCK inhibitor.

585 **Immunostaining.** 4% PFA-fixed cells were blocked and permeabilized with 5% goat serum + 1M  
586 Glycine + 1% Triton X-100 (all Sigma) in PBS without Ca and Mg or animal-free blocker (Vector  
587 Laboratories) + 1% Triton X-100 in milliQ water. All of the primary antibody information can be found  
588 in Supplementary Table 3. Staining was visualized using a Zeiss LSM780 confocal microscope.

589 **Histology analysis.** Paraffin embedding, paraffin block sectioning, and H&E staining were performed  
590 by the Pathology Core of The Centre for Phenogenomics.

591 **Quantitative PCR.** Gene expression analyses were completed as follows: RNA extraction by  
592 GenElute™ Mammalian Total RNA Miniprep Kit (Sigma), reverse transcription with QuantiTect  
593 Reverse Transcription Kit (Qiagen), Q-PCR with SensiFAST SYBR No-Rox Kit (Bioline) on Bio-Rad  
594 CFX Real-Time Systems (Bio-Rad), and analysis with Bio-Rad CFX Manager 3.1. All the information  
595 of primers and probes for the TaqMan Q-PCRs can be found in Supplementary Table 2. The reactions  
596 were performed using TaqMan Genotyping Master Mix (Thermo Fisher Scientific) and CFX Real-  
597 Time Systems, and were analyzed by CopyCaller Software v2.1 (Thermo Fisher Scientific).

598 **Luria and Delbruck assay.** The Luria and Delbruck assay was performed as previously described<sup>22</sup>.  
599 *CDK1*-TK homozygous 3C cells were single-cell plated in a 96-well plate using FACS. 21 single cell-  
600 derived cultures were grown to an average of 5 million cells per culture, and the number of single-  
601 positive cells in each culture were analyzed using flow cytometry. The mutation rate was calculated  
602 using the previously described equation<sup>23</sup> in <https://www.wolframalpha.com/>.

603 ***In vivo* transplantation of RPEs.** *CDK1*-TK homozygous 3C ES cells were transfected with PB-  
604 CAGGs-mCherry-pA plasmid and sorted for high expressors. 40,000 3C-derived RPEs only or 30,000  
605 3C-RPEs plus 10,000 mCherry-tagged 3C ES cells were injected subretinally with 0.5%/0.5% (wt/vol)  
606 hydrogel blend of hyaluronan and methylcellulose (HAMC) in HBSS. PBS or GCV (50 mg/kg)  
607 treatment were started the day after cell injection and were given every other day through  
608 intraperitoneal injections. Monitoring by funduscopy and optical coherence tomography were  
609 performed on the day after transplantation and then once a week.

610 **Monte Carlo simulation.** An ES cell population was considered as a mix of mutant and non-mutant  
611 cells with reference to the CDEL-SU locus (or loci). All possible mutations were categorized into three  
612 different types: type 1, when only the SU part of the locus becomes non-functional (*su1* allele); type 2,  
613 when both the CDEL and SU become non-functional (*su2* allele); type 3, when any of the above occurs  
614 as a result of LOH (Fig. 2a,b). Back mutations, such as *su1*→SU or *su2*→SU or *su2*→*su1*, were  
615 not considered, due to their extremely low probabilities (Fig. 2c). Back mutations, like SU/*su1* →  
616 SU/SU, SU/*su2* → SU/SU and *su1*/*su2* → *su1*/*su1*, were considered as a part of the more frequent LOH  
617 process. *p1*, *p2*, and *p3* were designated the probabilities of each mutation type, respectively. We  
618 distinguished between two types of *p3*: *p3mr* (probability LOH occurred through mitotic  
619 recombination), where both daughter cells survive; and *p3cnd* (probability LOH occurred through  
620 chromosomal non-disjunction), where one of the daughter cells with the single remaining copy of the  
621 chromosome is likely to die<sup>43</sup>. On the basis of these probabilities, matrices of transitions between all  
622 possible genotypes within one or two CDEL systems were constructed (Fig. 2c,  
623 <https://github.com/mashutova/failsafe>).

624 With each division cycle (*d*), all cells within the population except cells with the *su2*/*su2*  
625 genotype, were allowed to divide. Genotypes of *su1*/*su2* and *su1*/*su1* were considered escapees and the  
626 simulation initiated from one non-mutant cell.  $N(g1,d)$  was the number of cells of genotype *g1* at  
627 doubling *d*, and  $p(g1,g2)$  was the probability of transition from genotype *g1* to *g2*. In each doubling the  
628 number of cells changing genotype from *g1* to *g2* was determined through random sampling from a  
629 binomial distribution with parameters  $2*N(g1,d-1)$  and  $p(g1,g2)$ . We used Poisson approximation of  
630 binomial distribution to work with ultra-low  $p(g1,g2)$ . For each division, the number of cells of each  
631 genotype was assessed, and the simulation proceeded until the first escapee was detected.

632 For each starting genotype, we performed more than 10 million simulations and obtained a  
633 distribution of the number of doublings from the detection of the first escapee. On the basis of this data,  
634 we generated a function of FSL (overall number of trials divided by number of trials with escapees)  
635 over cell population size ( $2^d$ ) (Fig. 2d). Since all graphs contain almost linear regions, we used linear  
636 models to extrapolate them to high FSL values. To obtain linear regression lines, we only used  
637 simulated points from the linear-like part of the graph (*R*-squared > 0.999) with 95% confidence  
638 intervals less than 1000. To obtain a conservative boundary for the FSL, we used only the lowest CI  
639 values to build linear regressions.

640 To analyse the outcome from the aliquoting of the pool of fail-safe cells possibly containing  
641 escapees, using probability modelling we developed the following formula to calculate the drop of FSL  
642 (for details see Supplementary Calculation 1)

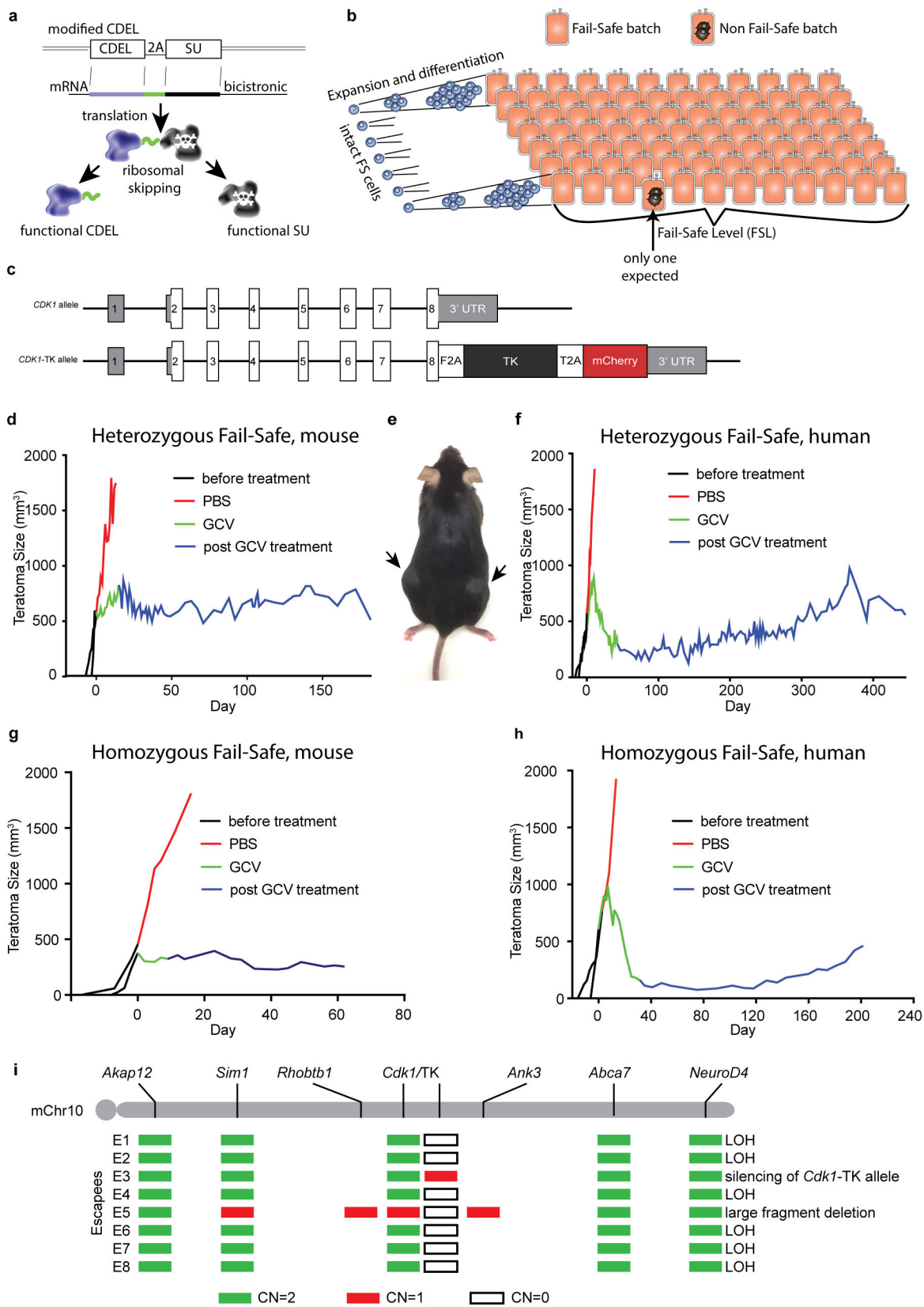
643 
$$\frac{FSL_{ap}}{FSL_a} \approx \frac{1}{A(1 - \sum_{k=0}^{m-1} 2^{-k-1} (\frac{A-1}{A})^{2^k})}$$

644 To reduce the complexity of the model, we considered only one escapee event in the pool, as  
645 the possibility of two independent escapees occurring in a pool is low in the quasi linear phase of FSL.  
646 Nevertheless, we tested the effect of this omission on the drop of FSL due to aliquoting using Monte  
647 Carlo simulation. We performed 10 million independent trials for a doubling of 20 and a doubling of  
648 27, and obtained a distribution of the number of escapees for each of them. Through randomly sampling  
649 a number of escapees from each trial to the A aliquots, we calculated the number of “bad” aliquots  
650 containing one or more escapees (Ab). To calculate a new FSL of the population after aliquoting, where  
651 FSLp is the FSL of the original population, we used the formula A\*FSLp/mean(Ab). The drop in FSL  
652 was measured *in silico* and was compared with the one we obtained from the equation obtained from  
653 the probability model.

654 **Data availability.** The DNA sequences of the vectors and plasmids used in this study are available  
655 upon request.

- 656  
657
- 658 39. Cong, L. *et al.* Multiplex Genome Engineering Using CRISPR/Cas Systems. *Science* **339**, 819–  
659 823 (2013).
  - 660 40. Behringer, R., Gertsenstein, M., Nagy, K. V. & Nagy, A. *Manipulating the Mouse Embryo*.  
661 (2013).
  - 662 41. Mereau, A., Grey, L., Piquet-Pellorce, C. & Heath, J. K. Characterization of a binding protein for  
663 leukemia inhibitory factor localized in extracellular matrix. *The Journal of Cell Biology* **122**, 713–  
664 719 (1993).
  - 665 42. Park, J., Kusminski, C. M., Chua, S. C. & Scherer, P. E. Leptin Receptor Signaling Supports  
666 Cancer Cell Metabolism through Suppression of Mitochondrial Respiration in Vivo. *The*  
667 *American Journal of Pathology* **177**, 3133–3144 (2010).
  - 668 43. Biancotti, J.-C. *et al.* The in vitro survival of human monosomies and trisomies as embryonic  
669 stem cells. *Stem Cell Research* **9**, 218–224 (2012).
- 670  
671

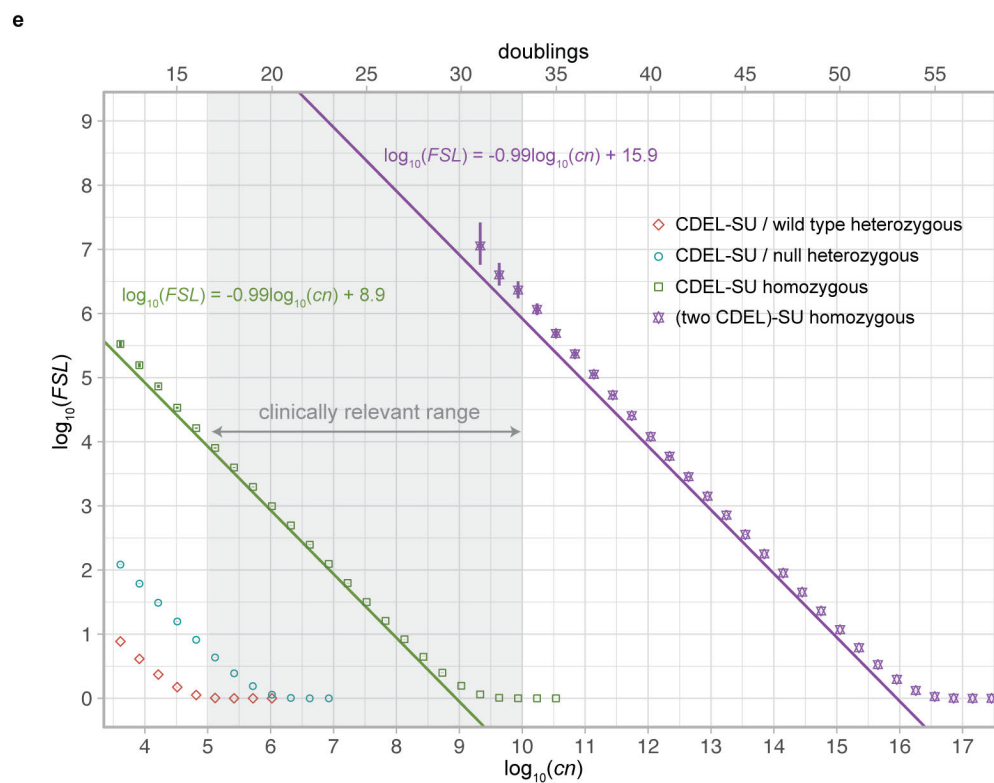
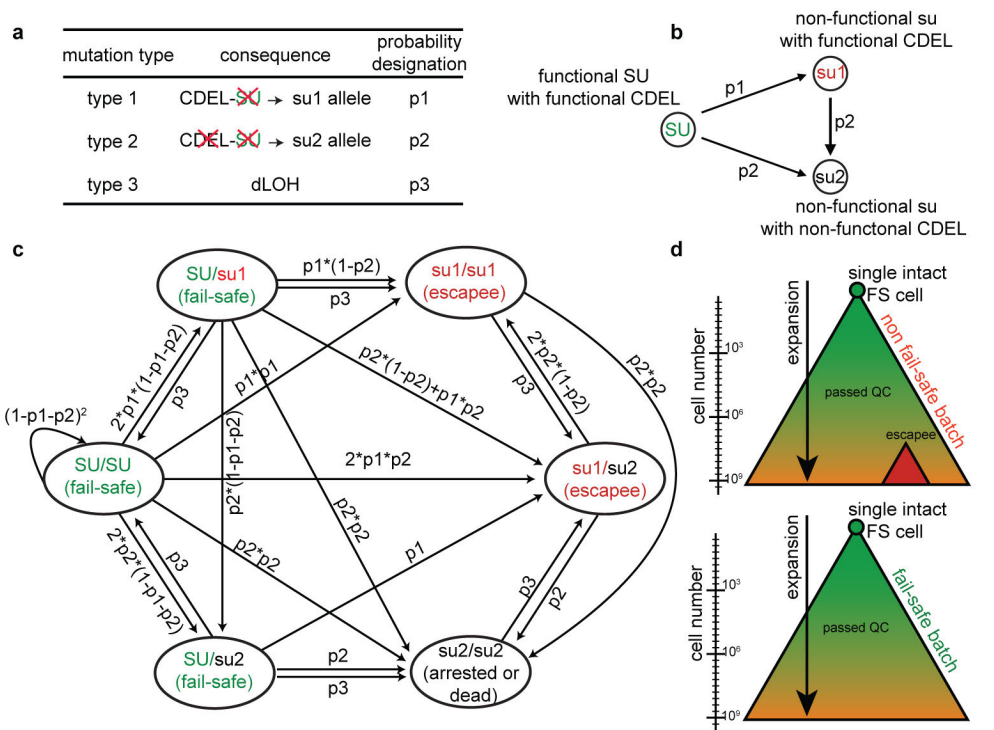




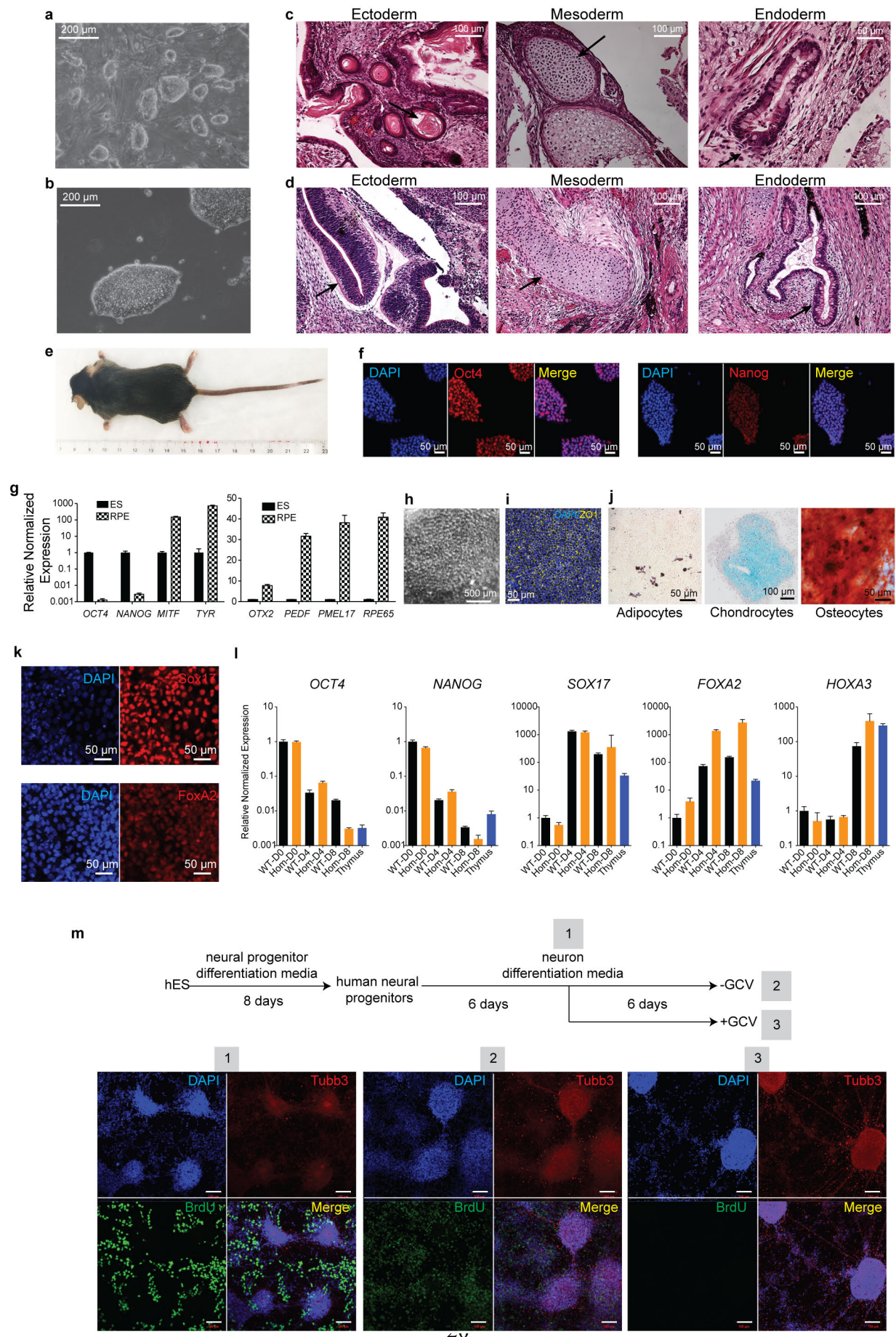
672  
673  
674  
675  
676

**Figure 1 | Fail-safe cell system: the concept, the definition, realization and properties.** **a**, The suicide gene is placed into a cell division essential locus (CDEL) resulting in a bicistronic mRNA that is translated into two proteins; a cell division essential factor and a drug-inducible suicide factor. **b**, Visual

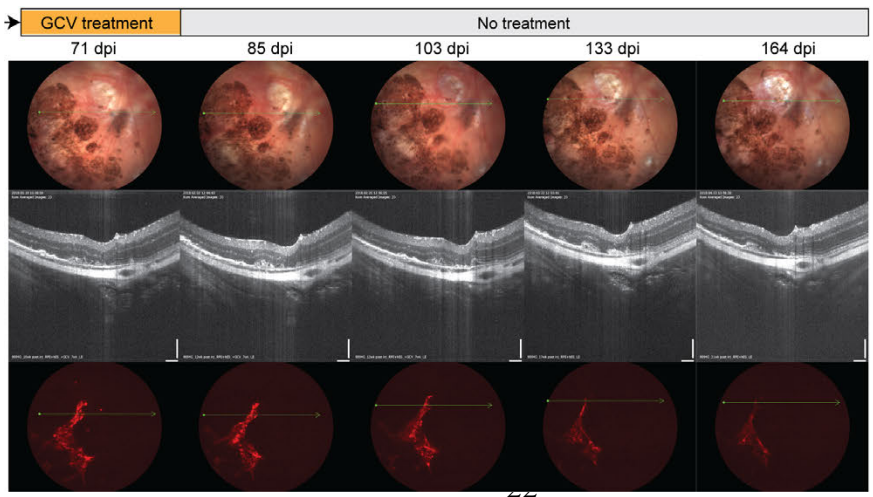
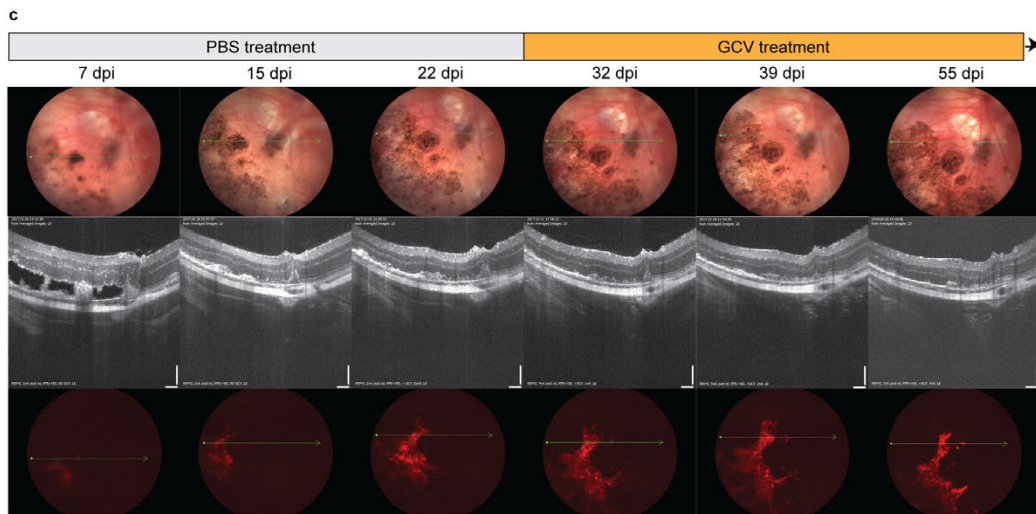
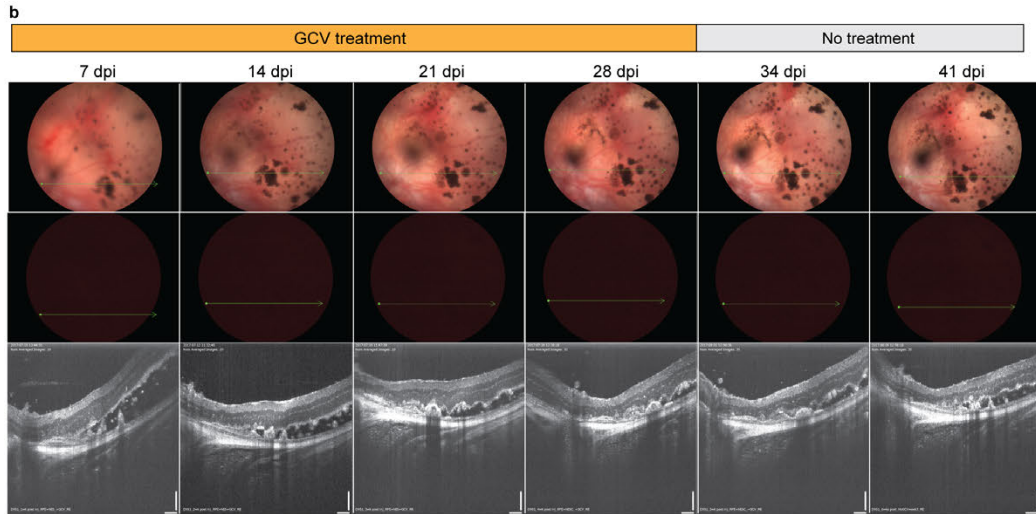
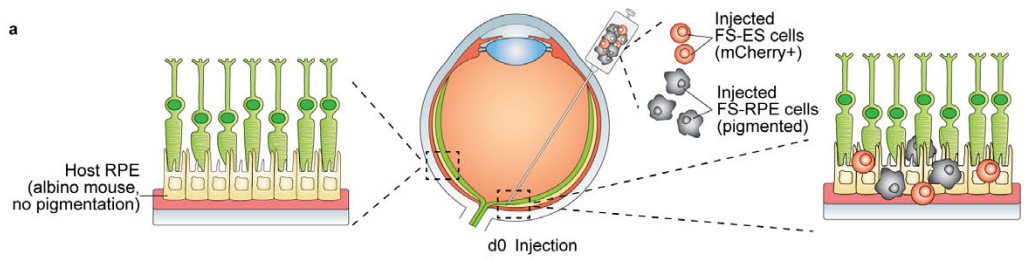
677 representation of the fail-safe level (FSL) defined by one non-fail-safe batch out of how many batches.  
678 **c**, The link between the prototype SU (HSV-TK) and the prototype CDEL (*CDK1*). **d**, Representative  
679 growth of teratomas formed by mouse *Cdk1*-TK/*Cdk1* cells, when the recipients were treated with PBS  
680 or GCV. **e**, Adult mouse with stabilized subcutaneous tissue (fail-safe ES cell-derived dormant teratoma)  
681 2.5 months after GCV treatment. **f**, Representative growth of teratomas formed by human *CDK1*-  
682 TK/*CDK1* ES cells, when the recipients were treated with PBS or GCV. **g**, Representative growth of  
683 teratomas formed by mouse *Cdk1*-TK/*Cdk1*-TK ES cells. **h**, Representative growth of teratomas formed  
684 by human *CDK1*-TK/*CDK1*-TKES cells **i**, Copy number analysis of mouse *Cdk1*-TK/*Cdk1* escapees  
685 identified in the experiment described in Extended Data Fig. 7.



687 **Figure 2 | Modelling the FS cell system and calculating FSL. a**, Three types of mutations that could  
688 affect the CDEL-SU allele. **b**, FS allele transition considered in the modelling and MC simulations. **c**,  
689 Genotype transition matrix considered in the modelling and MC simulations. **d**, Visual illustration of FS  
690 and non-FS batch formation during cell expansion. **e**, The function between therapeutic cell number and  
691 FSL determined by MC simulation (data points) for different initiating cell genotypes. Solid lines show the  
692 approximated linear regression on the “close to linear” part of the functions. The bars on certain data points  
693 represent the 95% confidence intervals of the FSL estimates. **f**, The drop of FSL due to aliquoting from a  
694 pool of cells relative to non-aliquoted batches of the same size.

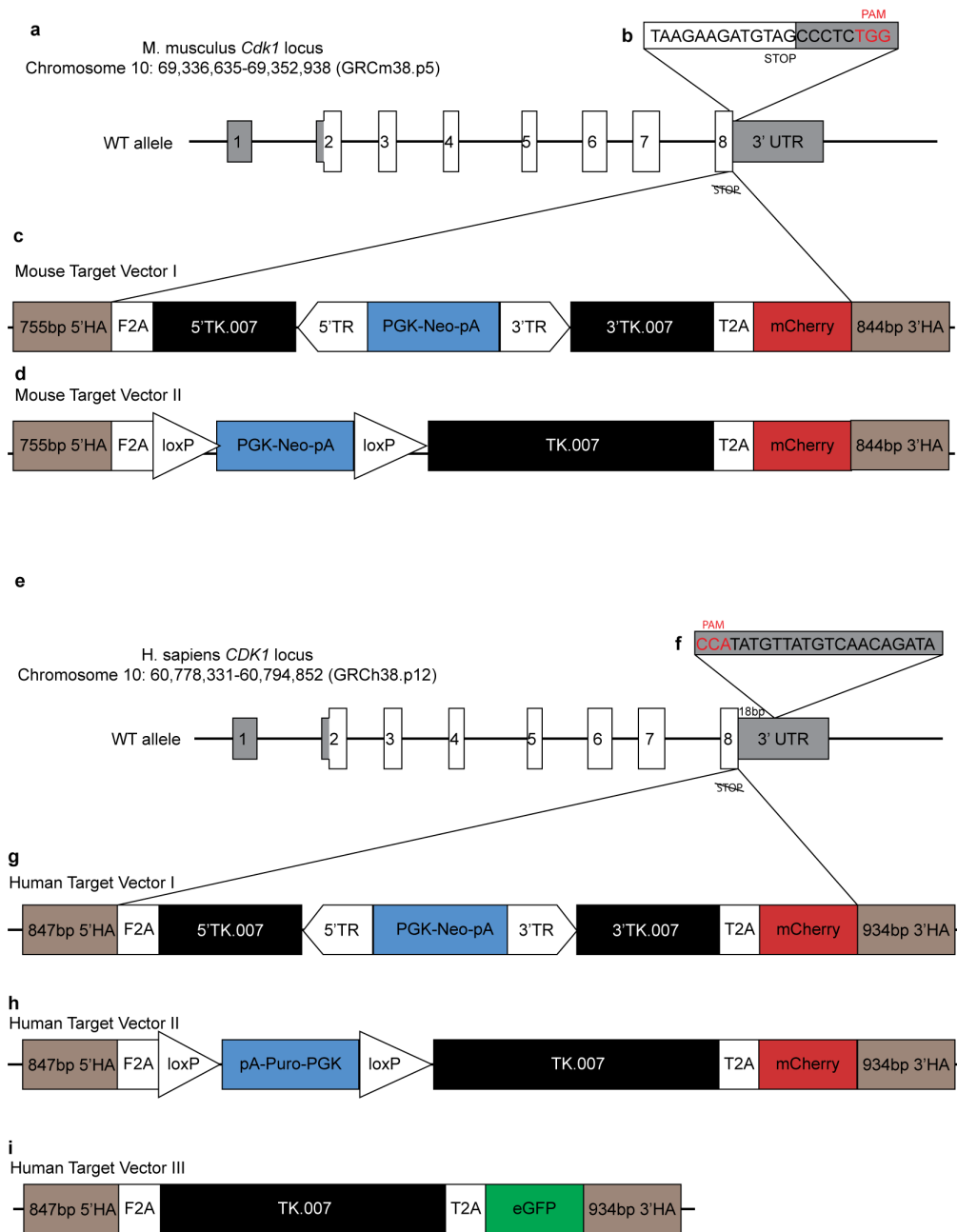


696 **Figure 3 | Mouse and human fail-safe homozygous *CDK1*-TK/*CDK1*-TK cells demonstrate**  
697 **pluripotency.** All experiments were performed using the same clone of mouse C2 or human H1 (Exc16-  
698 3C) *CDK1*-TK/*CDK1*-TK cells. **a**, Bright-field photograph showing mouse homozygous *Cdk1*-  
699 TK/*Cdk1*-TK ES cell morphology. **b**, Bright-field photograph showing human homozygous *CDK1*-  
700 TK/*CDK1*-TK ES cell morphology. **c**, H&E staining of a mouse *Cdk1*-TK/*Cdk1*-TK ES cell derived  
701 teratoma. **d**, H&E staining of a human *CDK1*-TK/*CDK1*-TK ES cell derived teratoma. **e**, An adult *Cdk1*-  
702 TK/*Cdk1*-TK mouse. **f**, OCT4 and NANOG staining of human *CDK1*-TK/*CDK1*-TK ES cells. **g**, Q-PCR  
703 characterization of *CDK1*-TK/*CDK1*-TK ES cell differentiation into RPE cells. Values represent mean  $\pm$   
704 SD, n = 3. **h**, Bright-field picture of human *CDK1*-TK/*CDK1*-TK ES cell derived RPE cells. **i**, ZO1  
705 staining of human *CDK1*-TK/*CDK1*-TK ES cell derived RPE cells. **j**, Human *CDK1*-TK/*CDK1*-TK ES  
706 cell derived adipocytes, chondrocytes and osteocytes. **k**, SOX17 and FOXA2 staining of human *CDK1*-  
707 TK/*CDK1*-TK ES cell derived definitive endoderm. **l**, *OCT4*, *NANOG*, *SOX17*, *FOXA2* and *HOXA3* Q-  
708 PCR characterization of ES cell (Day 0) differentiation into definitive endoderm (Day 4) and pharyngeal  
709 pouch endoderm (Day 8). Values represent mean  $\pm$  SD, n = 3. **m**, Human *CDK1*-TK/*CDK1*-TK ES cell  
710 differentiation into neural epithelial progenitors and subsequent neurons, with or without GCV  
711 treatment. Scale bar 100  $\mu$ m.



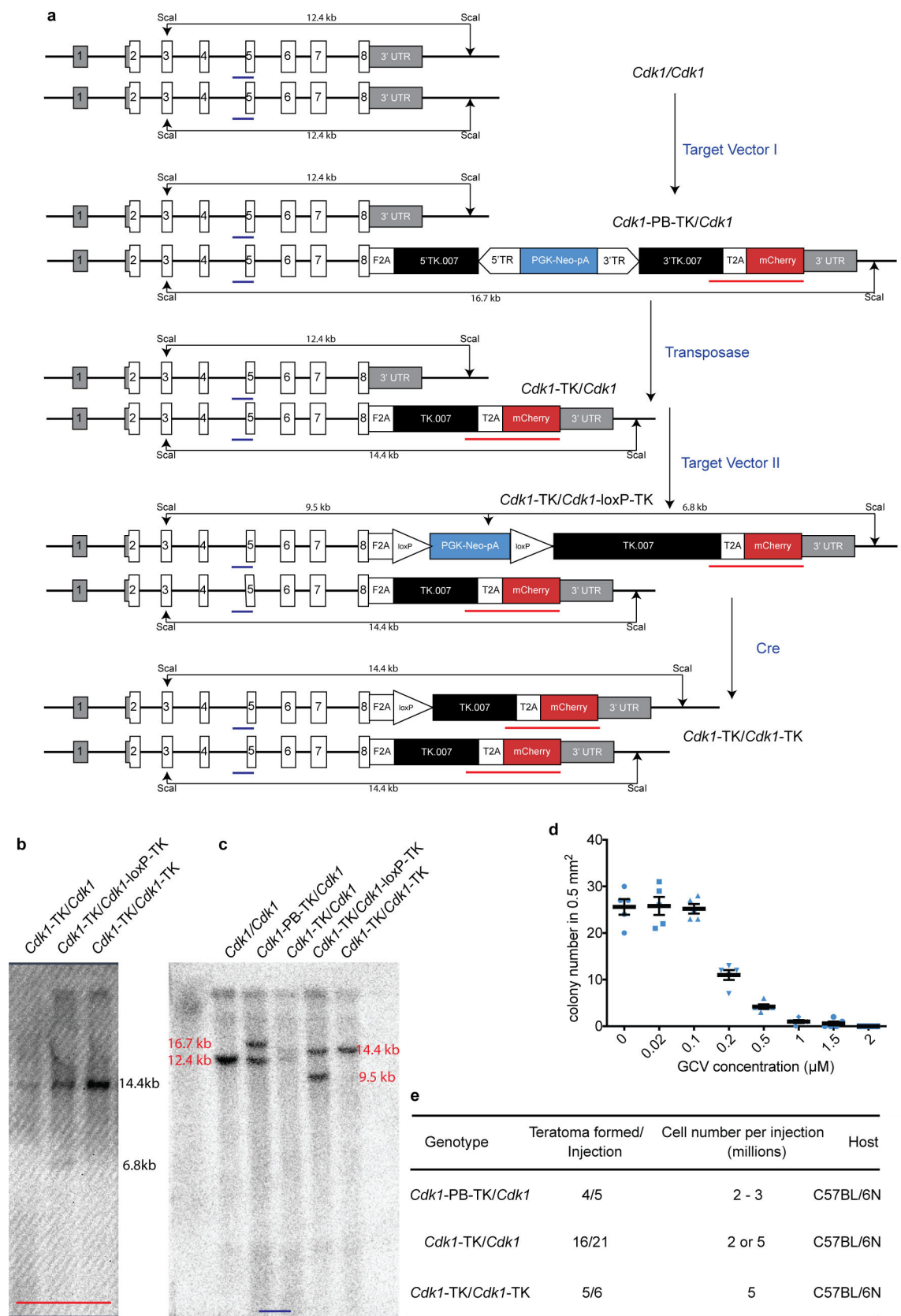
713 **Figure 4 | Fail-safe cell system in action; an *in vivo* proof of principle study.** **a**, A 3:1 mixture of  
714 human homozygous FS ES cell-derived RPE cells and homozygous FS ES cells were subretinally co-  
715 injected into NSG mice and imaged using funduscopy and optical coherence tomography (OCT)  
716 throughout GCV or PBS treatment. **b**, Funduscopy, OCT and fluorescence imaging of the eye receiving  
717 GCV treatment (4 weeks). **c**, Funduscopy, OCT and fluorescence imaging of the eye of the mouse that  
718 received PBS treatment (3 weeks) and developed an actively growing ES cell-derived lesion (mCherry+  
719 cells). dpi stands for days post injection.





720  
721

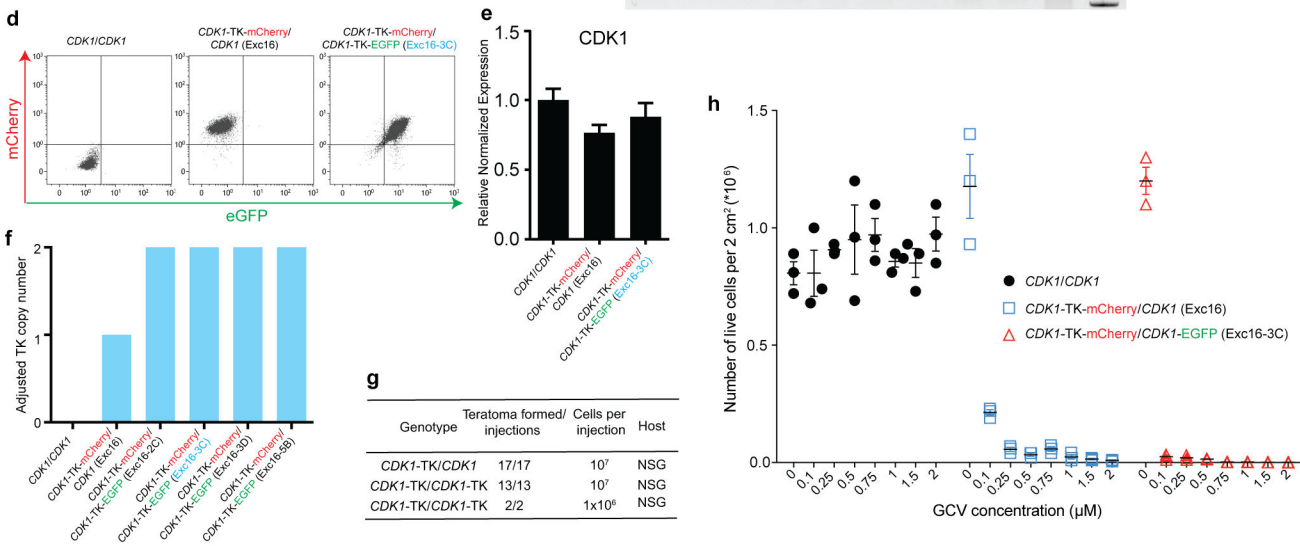
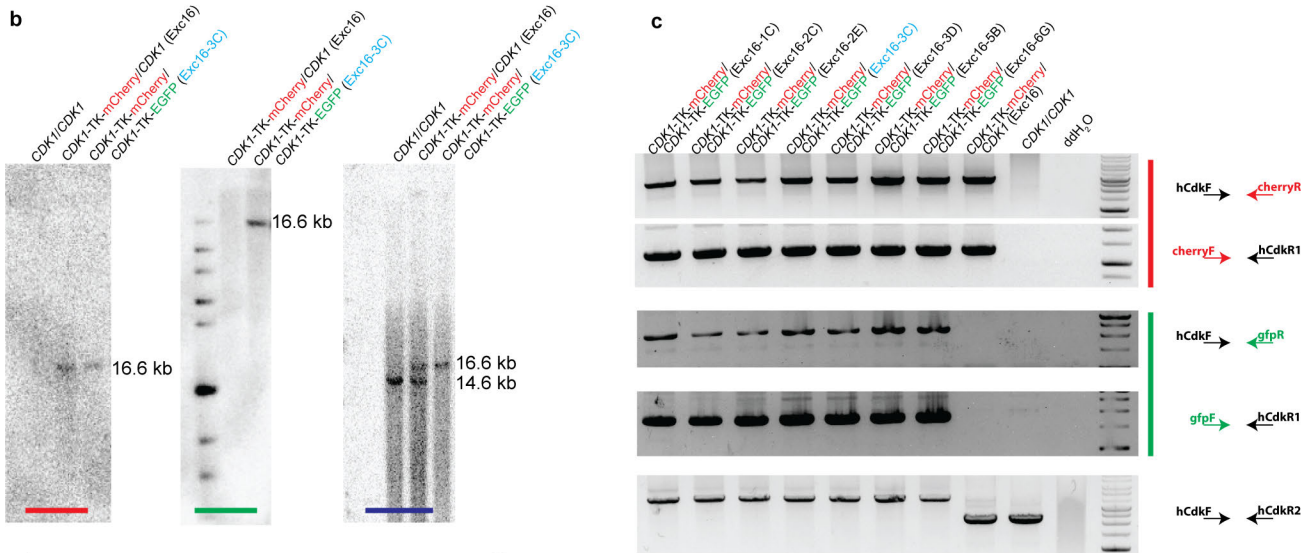
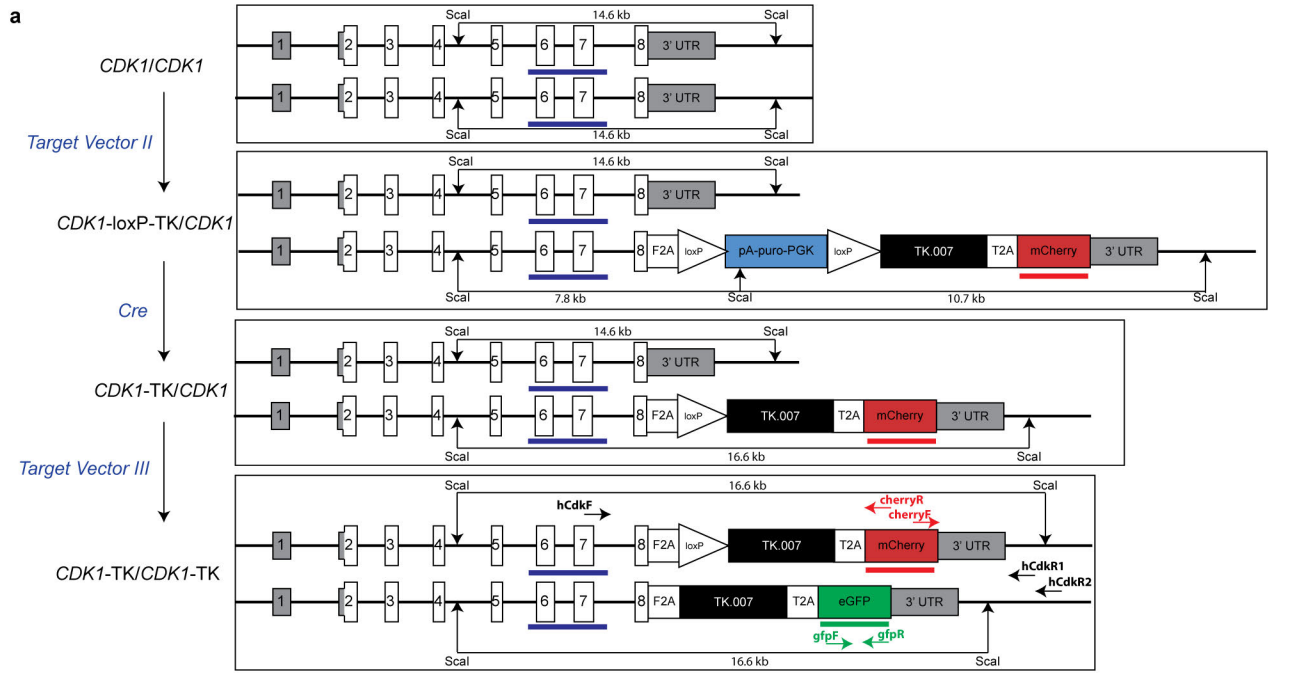
722 **Extended Data Figure 1 | Schematic of targeting vectors for mouse and human *CDK1*.** a, e, The  
723 genomic locus and structure of the mouse (a) and human (e) *CDK1* gene. b, f, CRISPR/Cas9 target site for  
724 mouse (b) and human (f) *CDK1*. c, d, g, h, i, The targeting vectors used in the study. The knock-in  
725 insertion replaced the *CDK1* stop codon with an F2A sequence, followed by the TK.007 linked to a  
726 fluorescent protein gene with a T2A sequence. Adding fluorescent reporters (mCherry and eGFP) to the  
727 insert permitted the visualisation of the modified *CDK1* allele expression in the cells. A positive selectable  
728 marker (neomycin or puromycin) was used to select for integration, and was subsequently removed by  
729 transiently expressing Cre recombinase or piggyBac (PB) transposase in the targeted cells, depending on  
730 the flanking loxP or PB terminal repeats (TR) in the target vector type, respectively. UTR: untranslated  
731 region, HA: homology arm, PGK: phosphoglycerate kinase, eGFP: enhanced green fluorescent protein,  
732 mCherry: mCherry fluorescent protein, pA: polyadenylation, Neo: neomycin selectable marker, Puro:  
733 puromycin selectable marker.



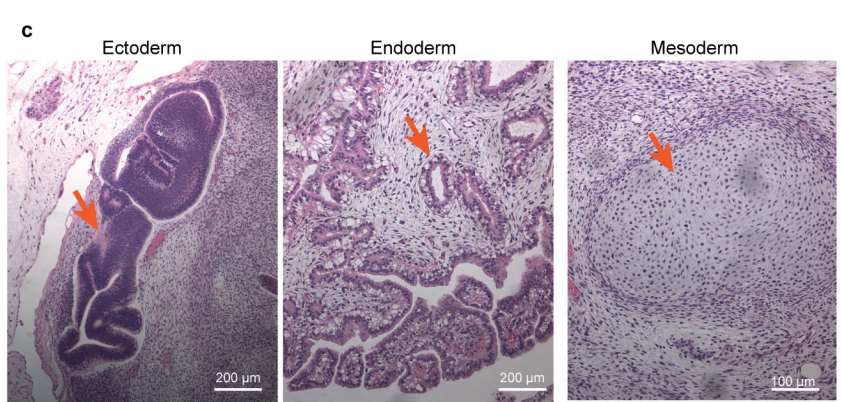
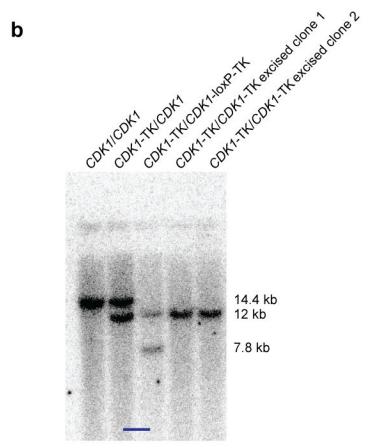
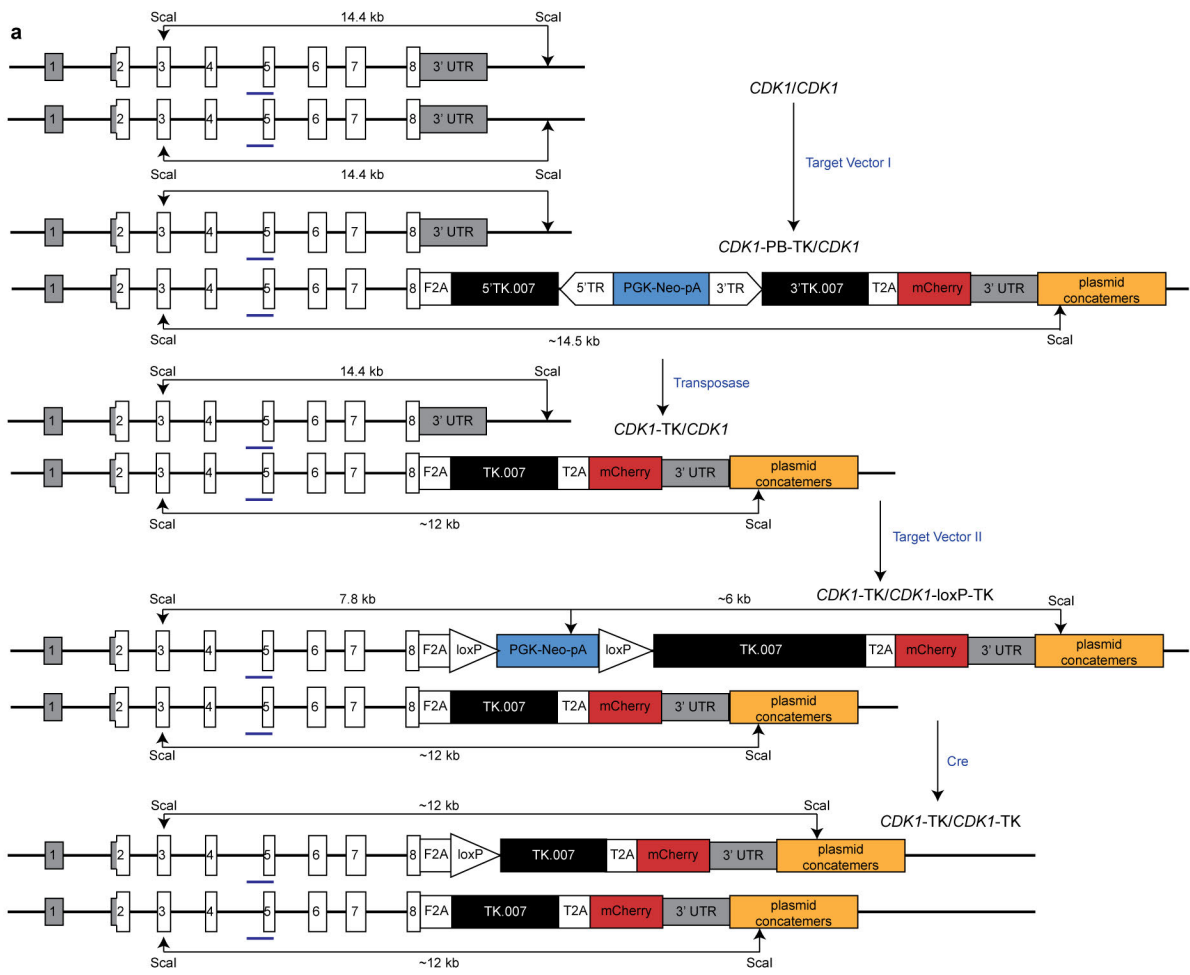
734  
735  
736  
737

**Extended Data Figure 2 | Generation, genotyping and characterization of mouse C57BL/6N C2 *Cdk1*-TK/*Cdk1* and *Cdk1*-TK/*Cdk1*-TK ES cells. a, Summary of the targeting steps used to generate**

738 mouse C2 *Cdk1*-TK/*Cdk1* and *Cdk1*-TK/*Cdk1*-TK ES cells. **b**, Southern blot genotyping with internal  
739 TK-mCherry probe. **c**, Southern blot genotyping with mouse *Cdk1* genomic probe. **d**, *In vitro* GCV  
740 dose-response killing curve of mouse C2 *Cdk1*-TK/*Cdk1* ES cells. **e**, Teratoma formation efficiency of  
741 mouse C2 *Cdk1*-PB-TK/*Cdk1*, *Cdk1*-TK/*Cdk1* and *Cdk1*-TK/*Cdk1*-TK ES cells.

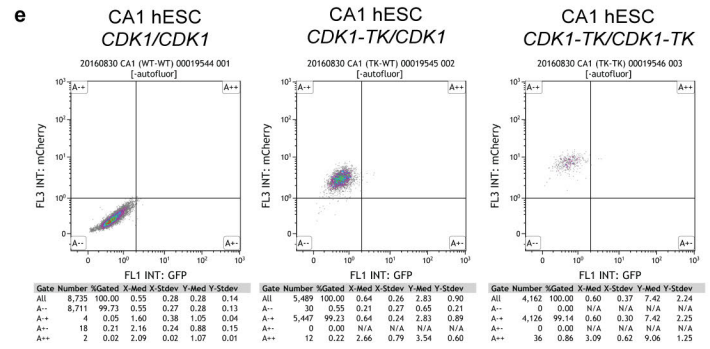


743 **Extended Data Figure 3 | Generation, genotyping and characterization of human H1 *CDK1-***  
744 ***TK/CDK1* and *CDK1-TK/CDK1-TK* ES cells. a,** Steps of generating human H1 *CDK1-TK/CDK1* and  
745 *CDK1-TK/CDK1-TK* ES cells. **b,** Southern blot genotyping of the *CDK1-TK/CDK1* clone Exc16 used  
746 in teratoma assays (Fig. 1c and Extended Data Fig. 7) and the *CDK1-TK/CDK1-TK* clone Exc16-3C  
747 used in the differentiation assays in Fig. 3. **c,** PCR genotyping of all the correct clones. **d,** Flow  
748 cytometry analysis of the *CDK1-TK/CDK1* clone Exc16 and the *CDK1-TK/CDK1-TK* clone Exc16-3C.  
749 **e,** SybrGreen Q-PCR of human *CDK1* expression in H1 WT, the *CDK1-TK/CDK1* clone Exc16 and the  
750 *CDK1-TK/CDK1-TK* clone Exc16-3C. Values represent mean  $\pm$  SD, n = 3. No significant difference  
751 among them. **f,** TaqMan Q-PCR copy number analysis of TKs of all the clones with the correct  
752 genotype. **g,** Table showing the efficiency of teratoma formation in NSG mice using H1 human ES cells.  
753 **h,** Dose-response analysis of wild type, *CDK1-TK/CDK1* and *CDK1-TK/CDK1-TK* human H1 ES cells.  
754 Cells were treated with different GCV concentrations, dissociated and counted after 7 days.

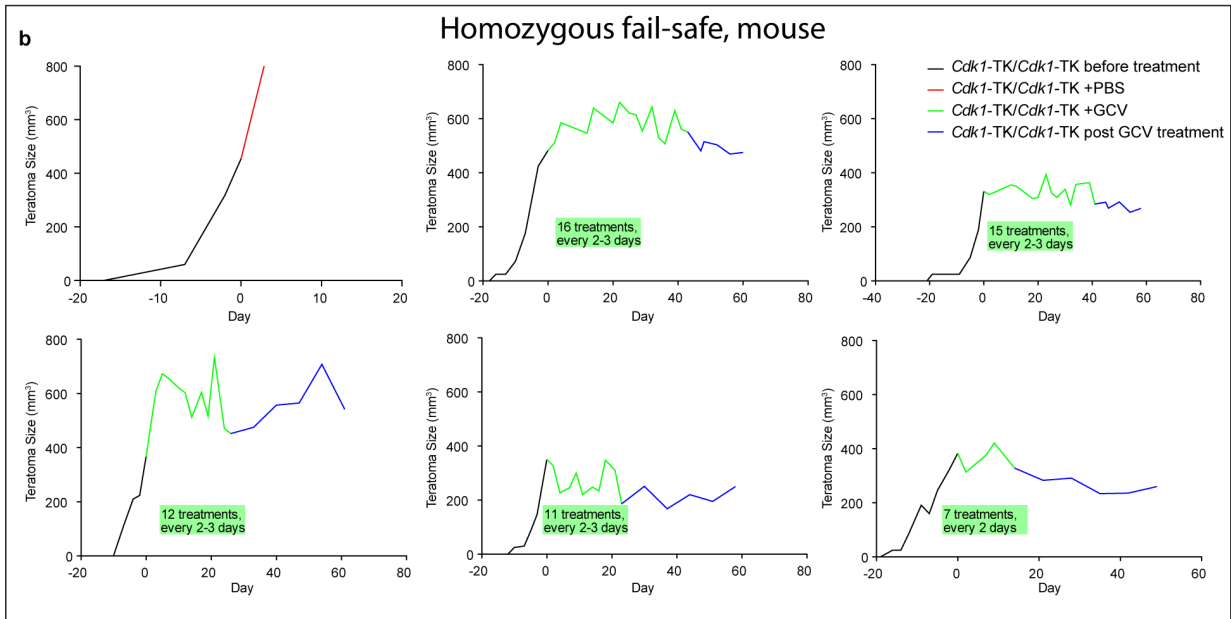
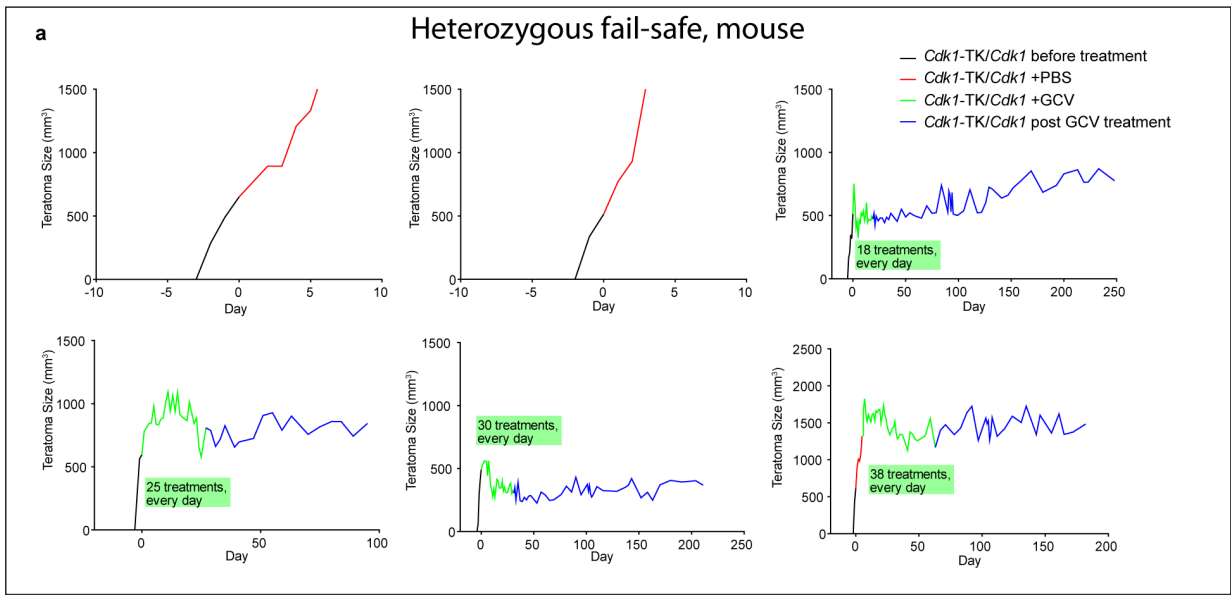


**d**

Genotype	Teratoma formed/ Injections	Cell number per injection	Host
CDK1-TK/CDK1-TK	4/4	1 - 4 x 10 <sup>6</sup>	NSG

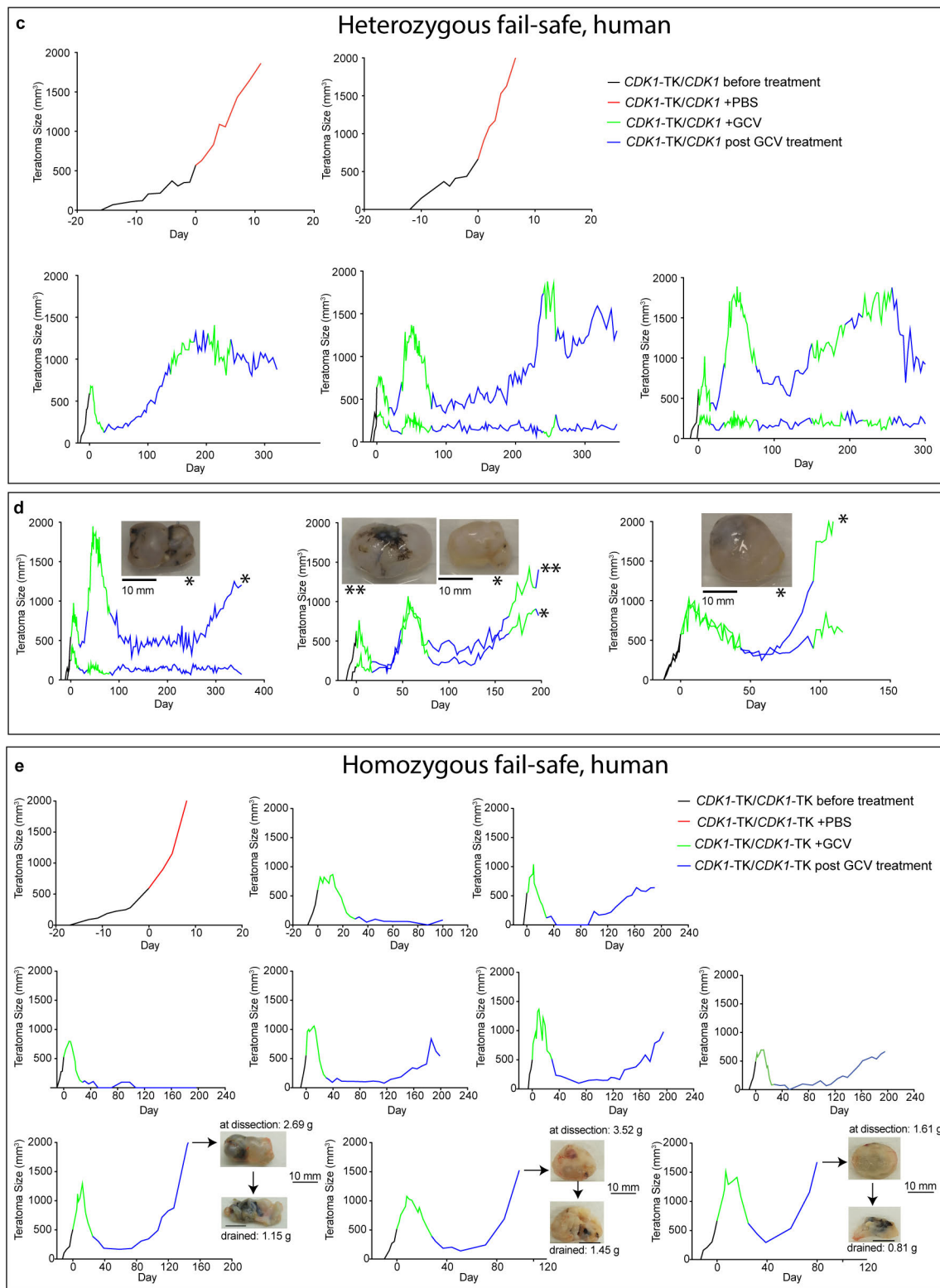


756 **Extended Data Figure 4 | Generation, genotyping and characterization of human CA1 *CDK1-***  
757 ***TK/CDK1* and *CDK1-TK/CDK1-TK* ES cells. a,** Steps of generating human CA1 *CDK1-TK/CDK1*  
758 and *CDK1-TK/CDK1-TK* ES cells. **b,** Southern blot genotyping of human CA1 *CDK1-TK/CDK1* and  
759 *CDK1-TK/CDK1-TK* ES cells. The plasmid concatemers are multiple copies of plasmid integration  
760 (including backbone). The Ampicillin gene in the backbone contains a *ScaI* restriction enzyme site  
761 which is consistent with the sizes of the band in southern blots. **c,** H&E staining of a *CDK1-TK/CDK1-*  
762 *TK* CA1 ES cell derived teratoma.



763

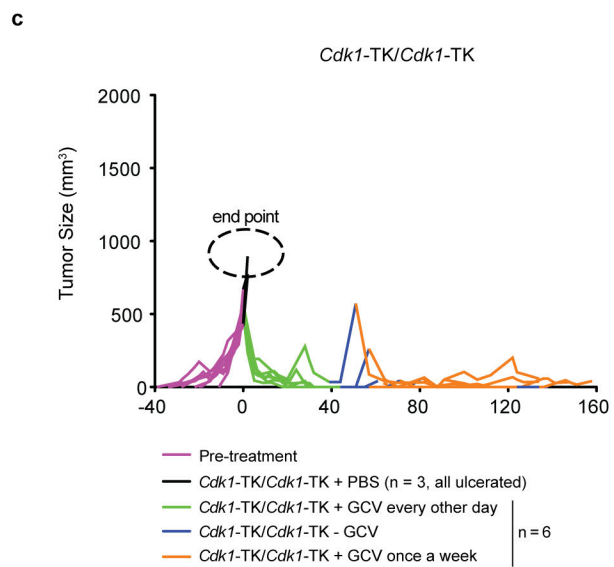
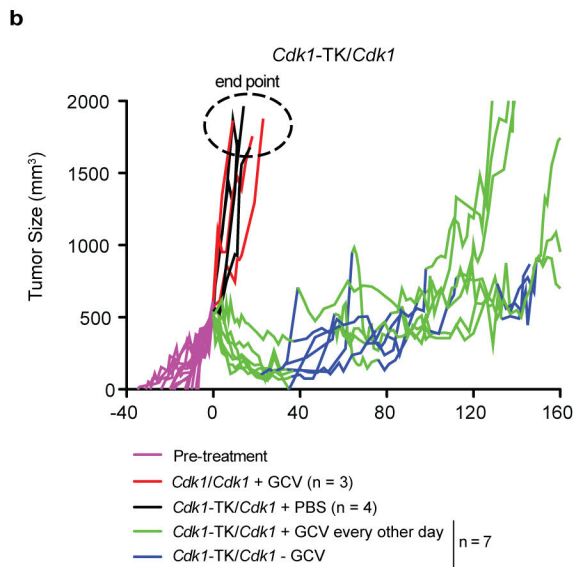
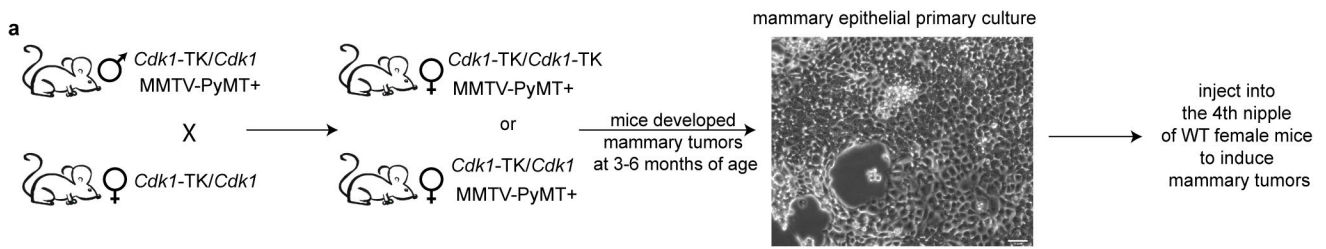




764  
765

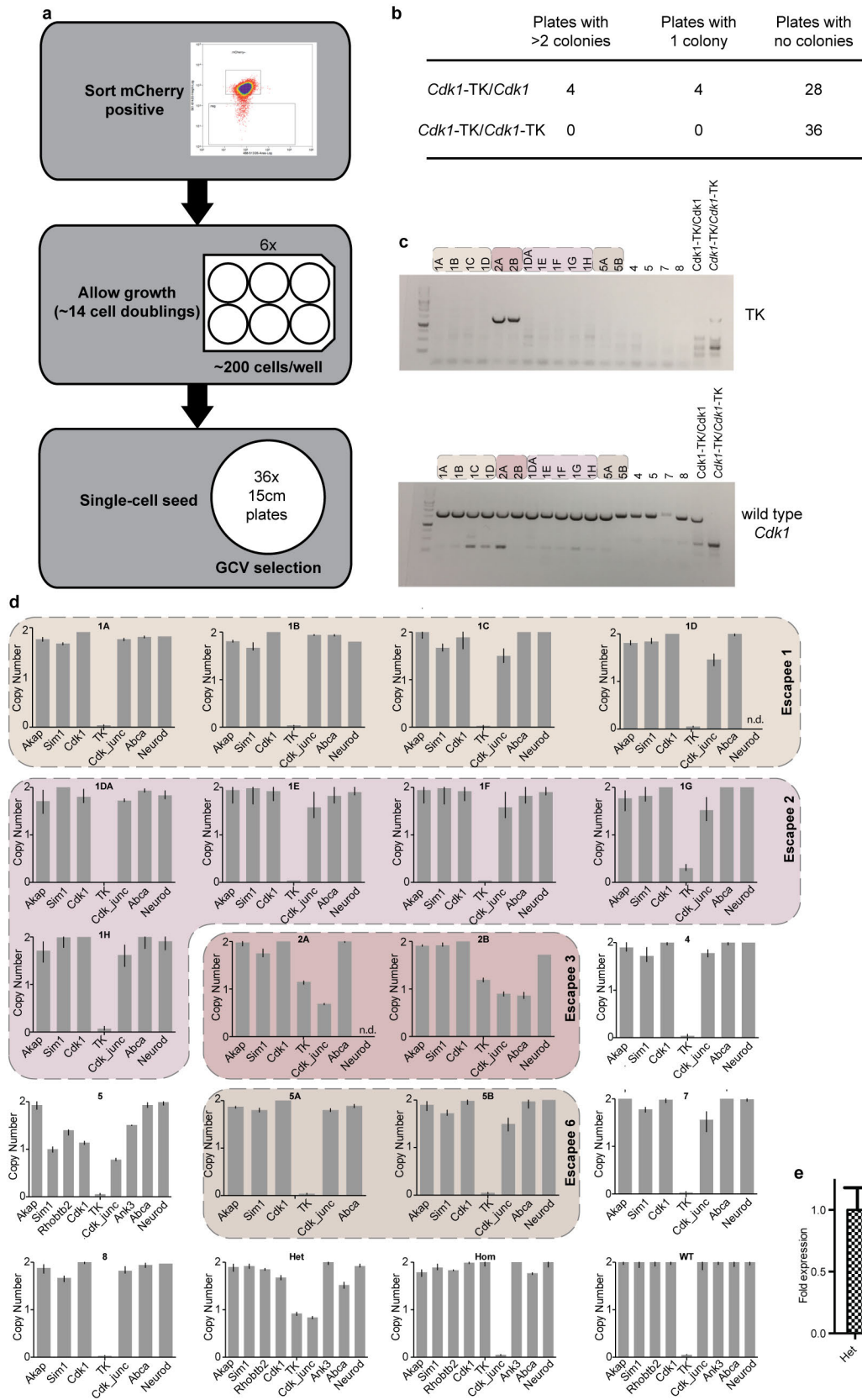
766 **Extended Data Figure 5 | Growth graphs of mouse and human ES cells-derived teratomas. a,**  
 767 **Growth of teratomas derived from mouse heterozygous fail-safe ES cells (*C2 Cdk1-TK/Cdk1*) b,**  
 768 **Growth of teratomas derived from mouse homozygous fail-safe ES cells (*C2 Cdk1-TK/Cdk1-TK*) c,**  
 769 **Growth of teratomas derived from human heterozygous fail-safe ES cells (H1 *CDK1-TK/CDK1*, clone**  
 770 **Exc16), daily GCV treatment. d, Examples of teratomas from human heterozygous fail-safe ES cells**

771 showing cyst formation, images of cystic teratomas at dissection are shown next to the corresponding  
772 growth line, daily GCV treatment. The graphs with two lines represent mice that had cells injected to  
773 both flanks. The graphs with one line represent mice that had cells injected to one flank. The GCV  
774 treatment regime varies among mice because each teratoma behaves differently; we started GCV when  
775 the teratoma size started to increase. **e**, Growth of teratomas derived from human homozygous fail-safe  
776 ES cells (H1 *CDK1-TK/CDK1-TK*), GCV treatment was every other day. Images of cystic teratomas are  
777 shown next to the corresponding growth line, cysts were drained after dissection to show the difference  
778 in tumour weight due to the fluid present in the tissue. Each graph represents one mouse.



779  
780

781 **Extended Data Figure 6 | Breast cancer transplantation assay using heterozygous and homozygous**  
 782 **FS mammary tumour cells.** **a**, Generation of mouse line and experimental design. **b**, Growth of  
 783 mammary gland tumours derived from mouse *Cdk1/Cdk1* and *Cdk1-TK/Cdk1* mammary epithelial cells  
 784 with PBS or GCV treatment. **c**, Growth of mammary gland tumours derived from mouse *Cdk1-TK/Cdk1-*  
 785 *TK* mammary epithelial cells with PBS or GCV treatment.



786  
787

788 **Extended Data Figure 7 | *In vitro* experiments with mouse *Cdk1-TK/Cdk1*, *Cdk1-TK/Cdk1-TK* ES**  
789 **cells and subsequent characterization of escapees. a**, Experimental design: mCherry+ cells were

790 selected by sorting to ensure that the starting cell population did not contain escapees. These cells were  
791 plated on 6 well plates (200 cells/well, 36 total wells) and allowed to grow to 14 cell doublings (this was  
792 estimated by counting cells in sample wells). The 36 cultures were then resuspended to a single-cell  
793 suspension and each was plated to a 15 cm plate ( $4 \times 10^6$  cells). One day after plating, selection with GCV  
794 was started and maintained until escapee colonies appeared. **b**, Escapee numbers obtained in 36  
795 independent cultures growing from *Cdk1*-TK/*Cdk1*, *Cdk1*-TK/*Cdk1*-TK ES cells. **c**, PCR to determine the  
796 presence of TK. **d**, TaqMan copy number Q-PCR analysis of *Akap*, *Sim1*, *Cdk1* junction of exon 8 and  
797 3'UTR, *Neurod*, *Cdk1*, *TK*, *Abca* on mouse Chr. 10. Values represent the copy number calculated by  
798 CopyCaller Software v2.1 and the bars indicate the range from the minimum to the maximum number. n =  
799 3. The same color in the background of **c** and **d** indicates that they are from the same independent culture.  
800 **e**, Q-PCR to compare TK expression level in *Cdk1*-TK/*Cdk1* escapee clone 2A and C2 WT ES cells.  
801 Values represent mean  $\pm$  SEM. n = 3.

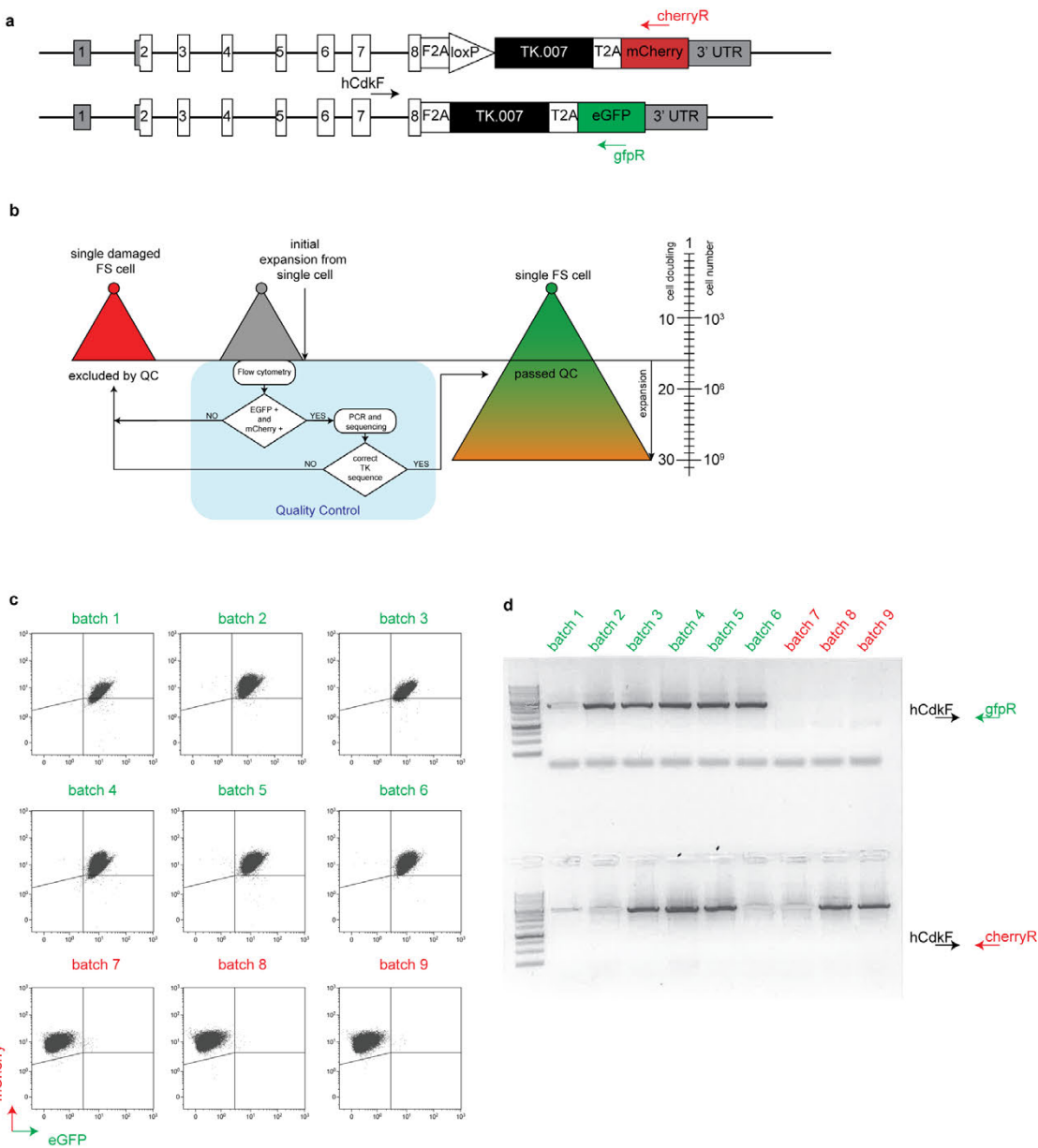
a

Number of replicate culture	Initial number of cells per culture	Average number of cells/culture	Total numbers of cells	Total live cells analyzed	Live cells / total cells	Average mutants per sample	LOH rate per cell division
21	1	4.9x10 <sup>6</sup>	4.9x10 <sup>6</sup> x21= 1.029x10 <sup>8</sup>	18,833,305	0.18	eGFP only: 303	mCherry loss frequency: 9.05x10 <sup>-6</sup>
						mCherry only: 251	eGFP loss frequency: 7.68x10 <sup>-6</sup>

b

Samples	All events	Live cells	Single cells	eGFP+ mCherry-	mCherry+ eGFP-
1	50,000	36,102	14,261	0	1
2	1,387,922	1,166,927	663,704	11	32
3	1,306,685	1,229,940	734,030	59	95
4	1,977,744	1,473,607	1,229,131	29	38
5	2,492,764	2,051,819	1,798,915	114	114
6	2,639,618	2,160,508	1,891,409	102	108
7	559,819	406,149	374,528	18	3
8	39,161	15,380	12,977	0	1
9	1,661,726	1,354,148	1,153,558	156	81
10	2,315,402	1,911,681	1,664,292	63	75
11	843,549	611,761	529,324	124	45
12	2,088,898	1,595,412	1,337,789	86	69
13	2,468,994	1,853,728	1,628,365	69	75
14	92,019	56,795	46,791	10	9
15	1,791,662	1,076,661	953,464	7	4
16	2,153,934	1,680,018	1,485,732	179	106
17	1,416,523	1,029,636	882,532	7	8
18	1,096,211	771,314	653,076	32	25
19	15,695	8,297	6,665	1	0
20	764,311	598,206	533,928	28	6
21	1,802,185	1,369,832	1,238,834	72	73
<b>Total</b>	<b>28,964,822</b>	<b>22,457,921</b>	<b>18,833,305</b>	<b>1,167</b>	<b>968</b>
Total mutants in all samples				6,376.16	5,288.89
Average mutants per sample				303.62	251.85
Mutation rate				9.05x10 <sup>-6</sup>	7.68x10 <sup>-6</sup>

802  
803804 **Extended Data Figure 8 | Calculation of the LOH rate at the human *CDK1* locus with human H1**  
805 ***CDK1-TK/CDK1-TK* ES cells. a, Summary table. b, Detailed cell number for each individual clone.**

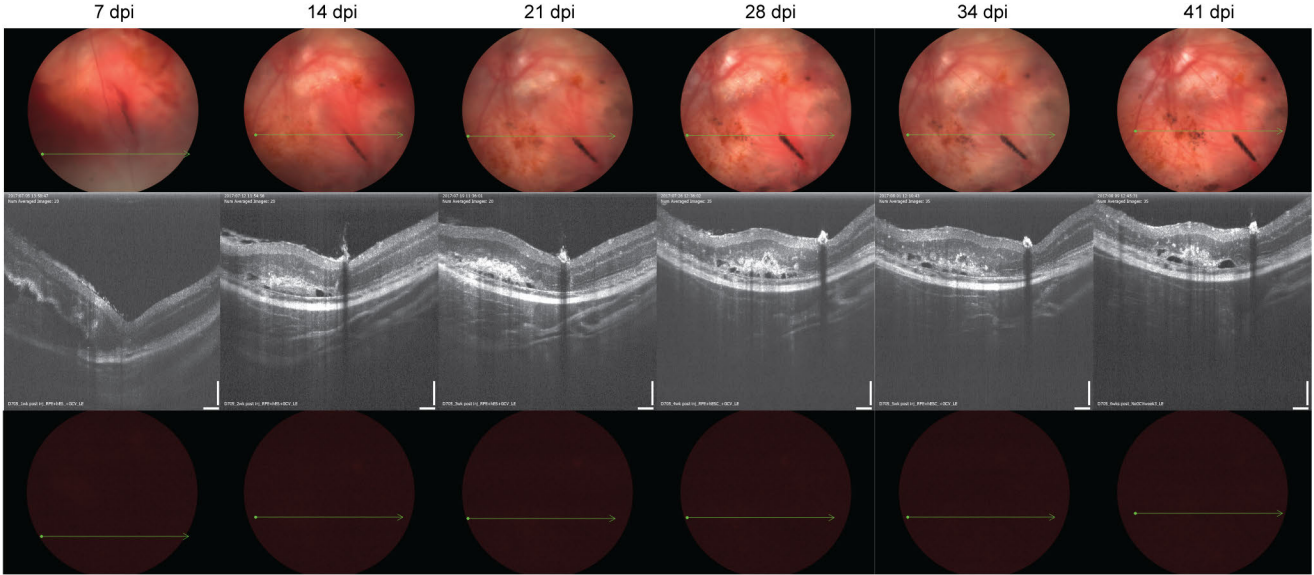
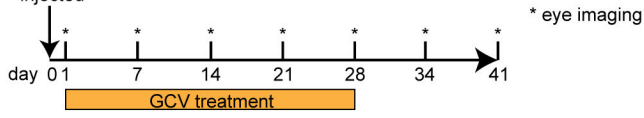


806  
807  
808  
809  
810  
811

**Extended Data Figure 9 | Quality control (QC) of batches generated from single human H1 *CDK1-TK/CDK1-TK* ES cells.** **a**, Schematics of the alleles in the *CDK1-TK/CDK1-TK* human ES cells used in the quality control. **b**, Workflow schematic of performing QC on several ES cell batches. **c**, An example of the flow cytometry for the QC of nine clonally derived batches. **d**, An example of PCR for the QC of nine clonally derived batches.

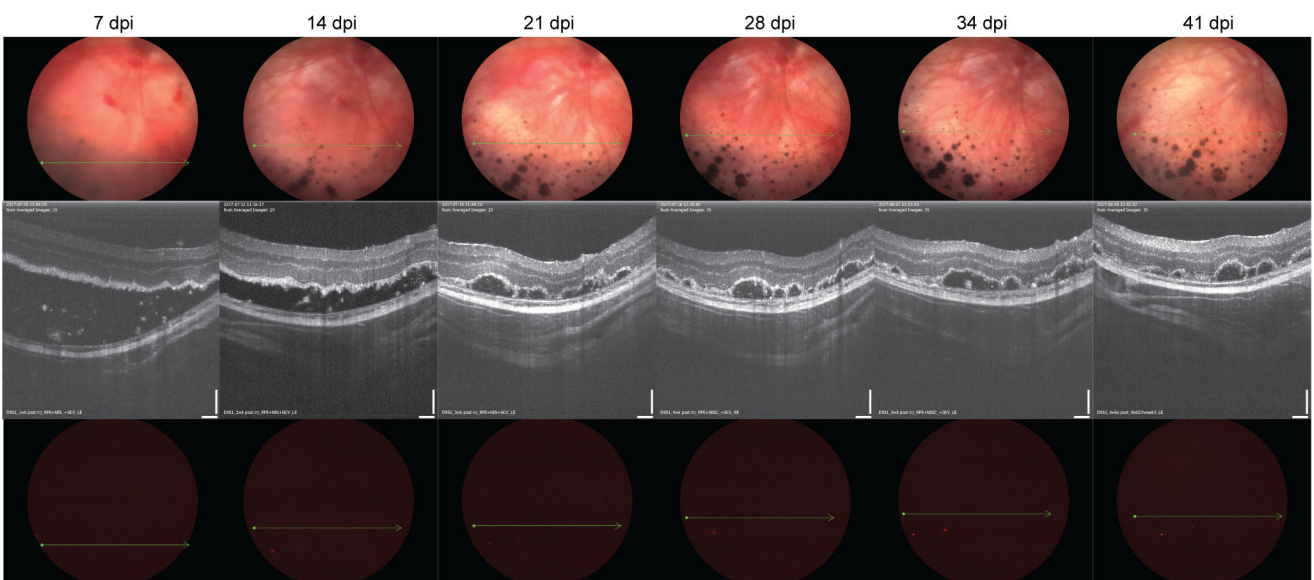
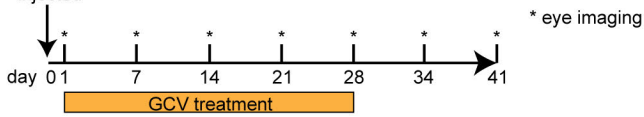
**a**

3x10<sup>4</sup> FS-RPE cells +  
1x10<sup>4</sup> FS-ES cells  
injected



**b**

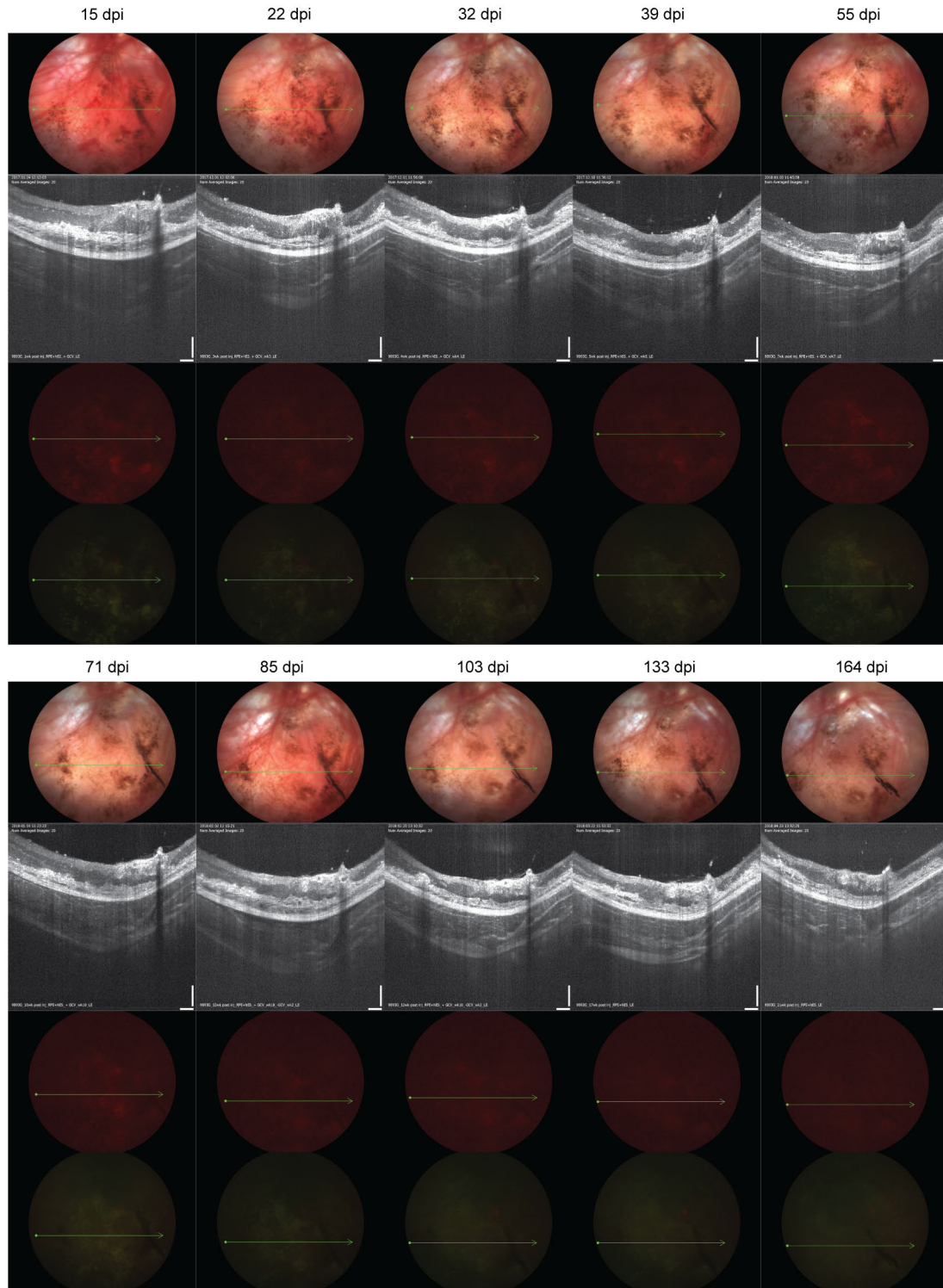
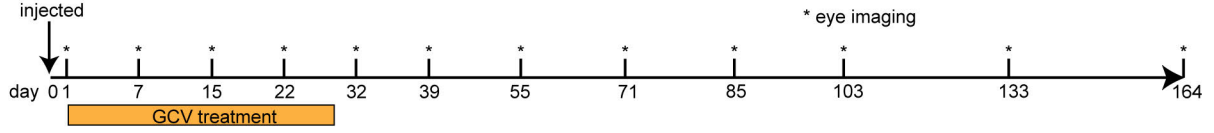
3x10<sup>4</sup> FS-RPE cells +  
1x10<sup>4</sup> FS-ES cells  
injected



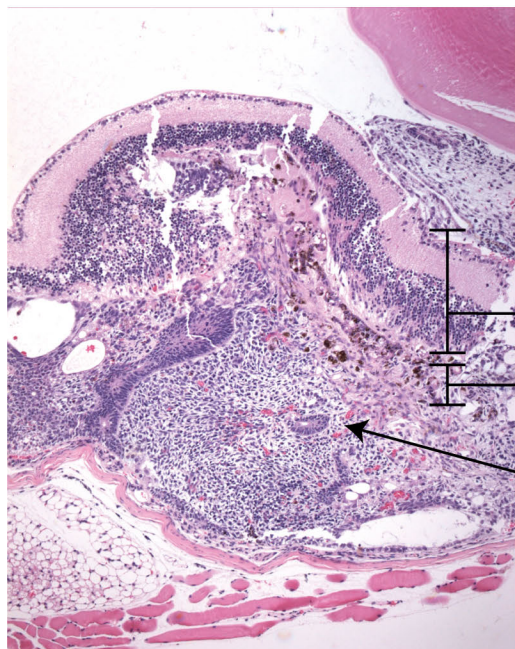


c

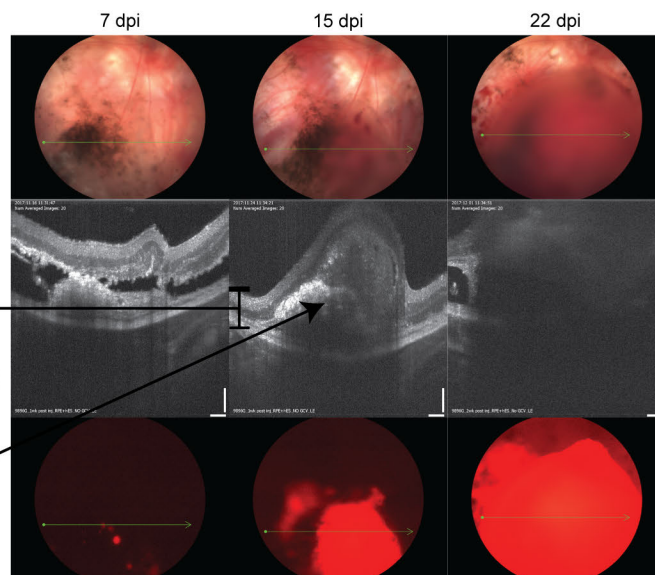
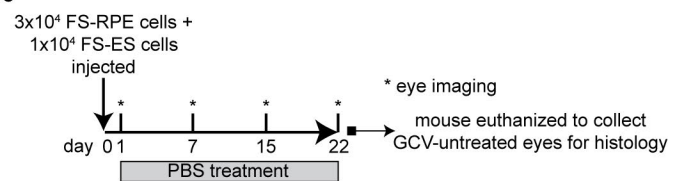
$3 \times 10^4$  FS-RPE cells +  
 $1 \times 10^4$  FS-ES cells  
injected



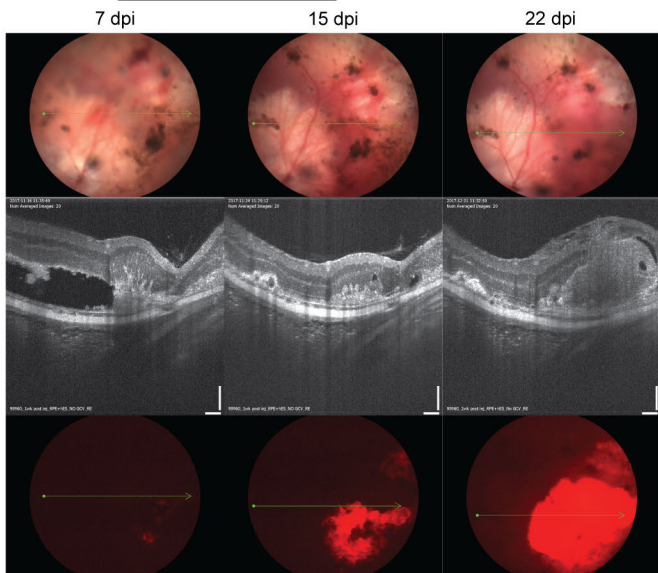
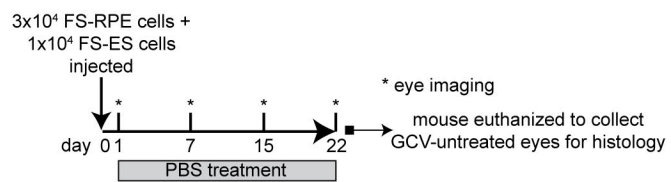
**d**



**e**

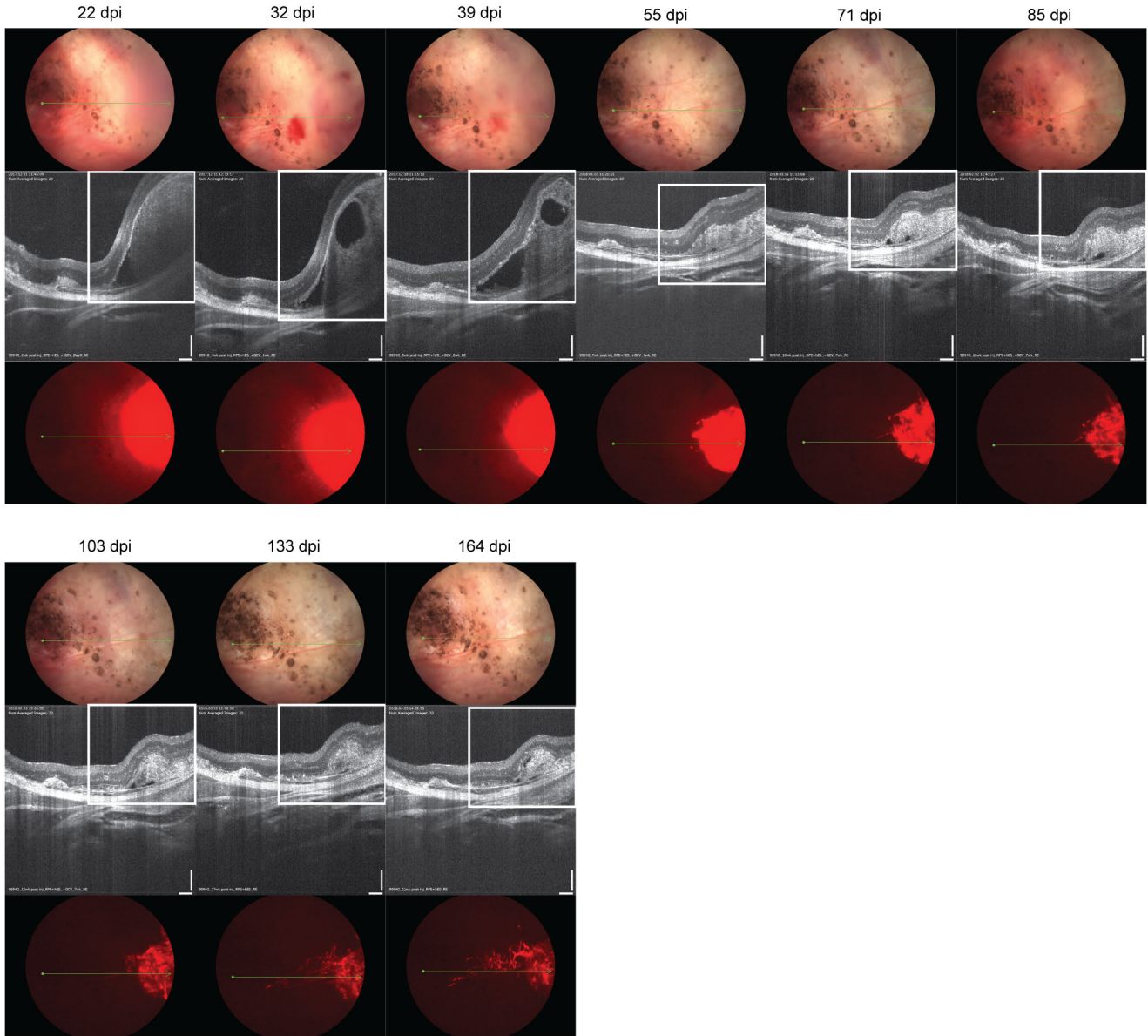
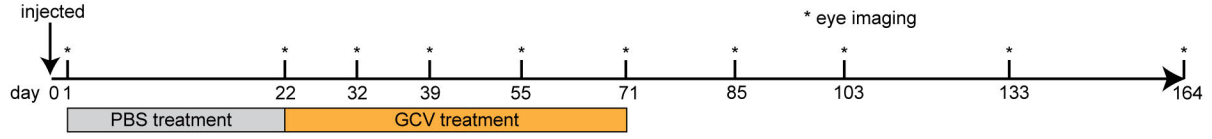


**f**



**g**

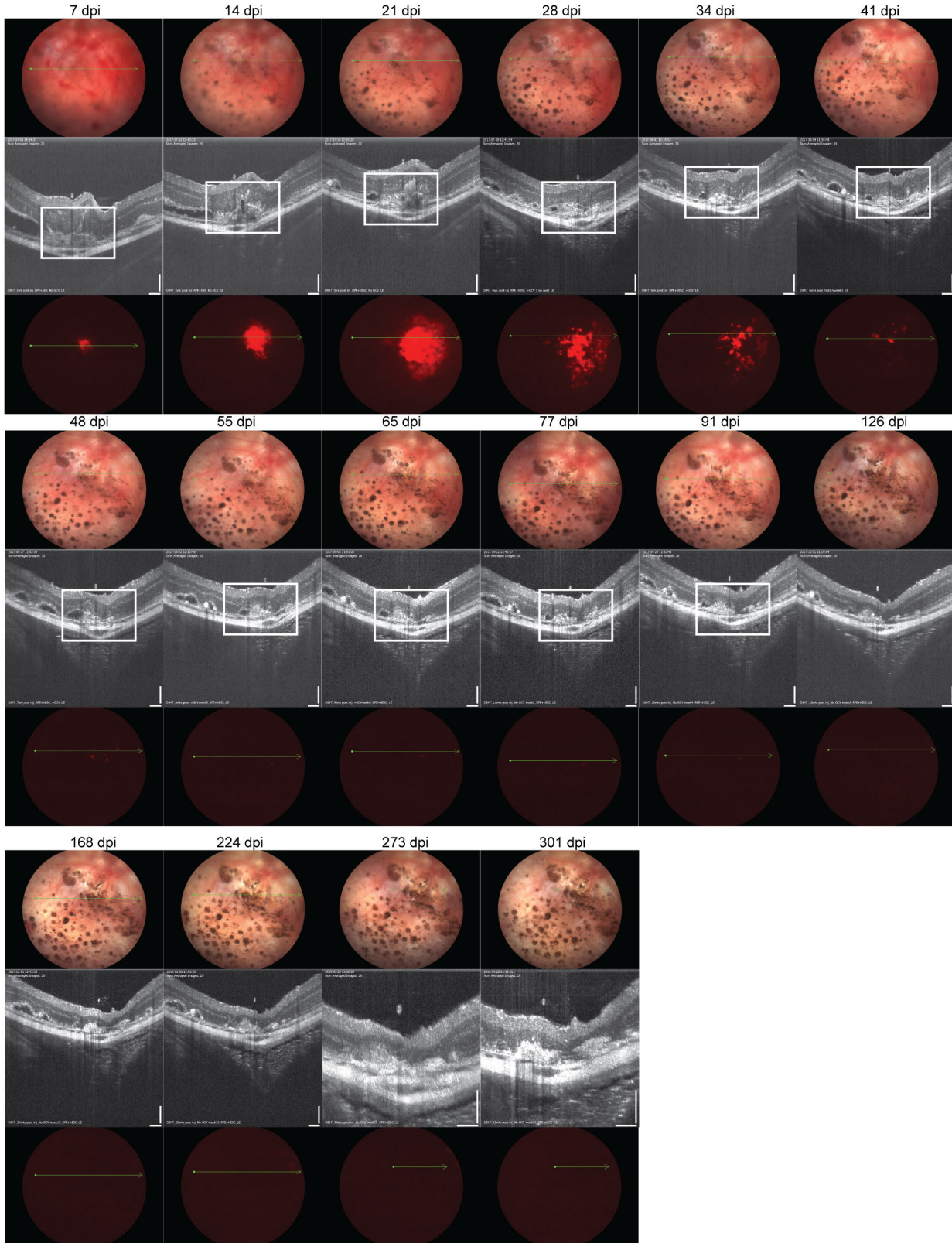
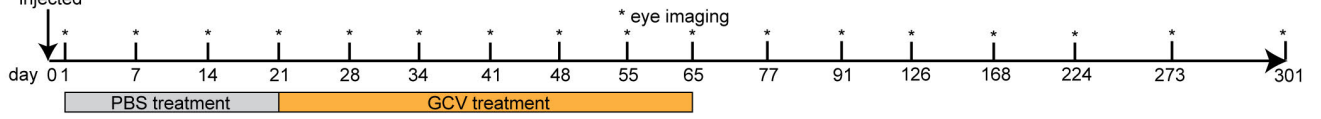
3x10<sup>4</sup> FS-RPE cells +  
1x10<sup>4</sup> FS-ES cells  
injected



816

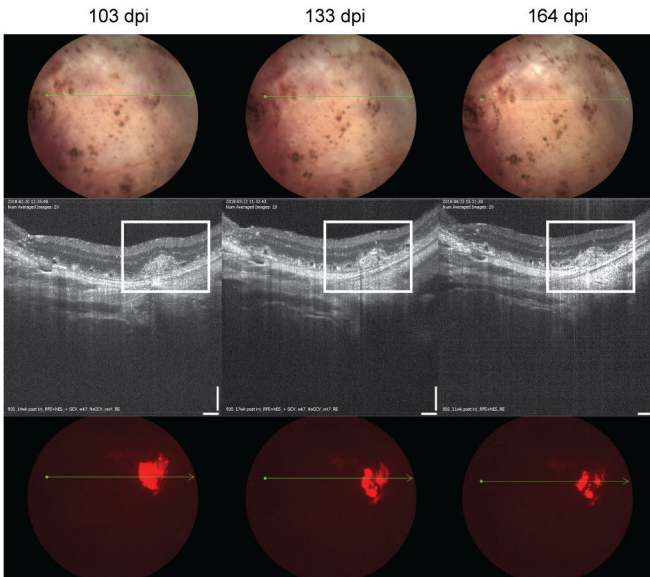
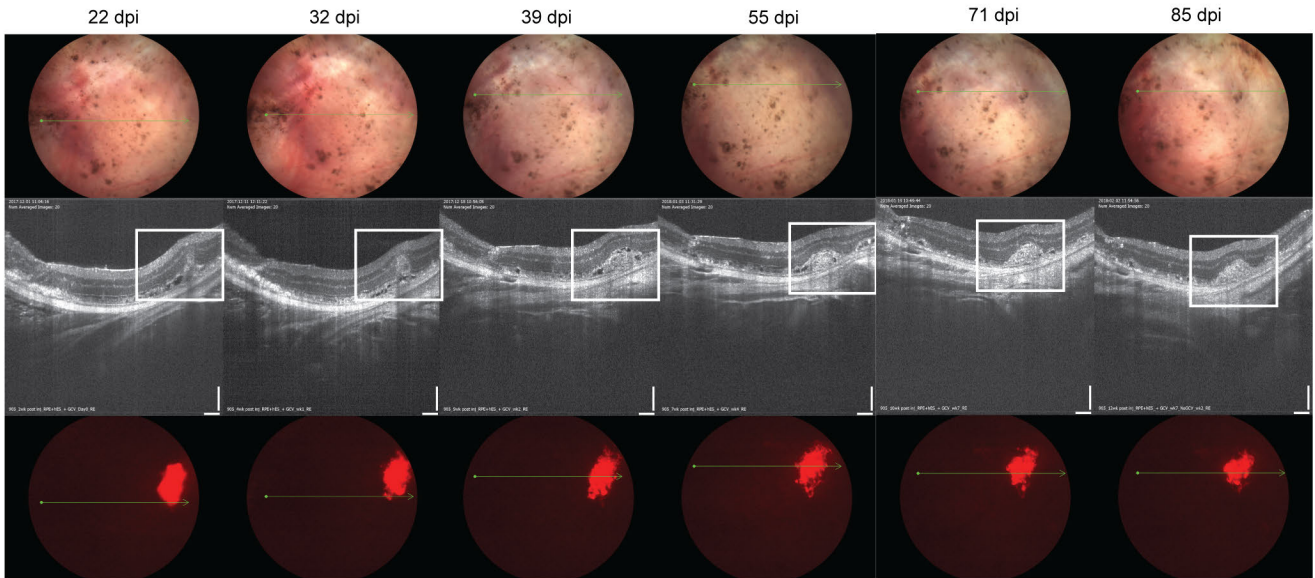
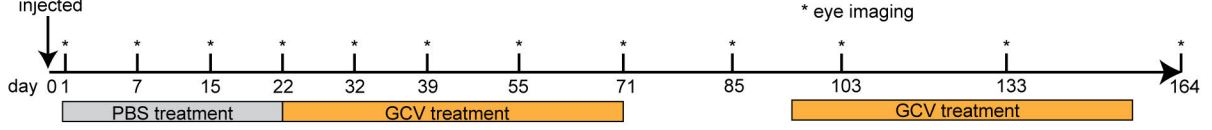
h

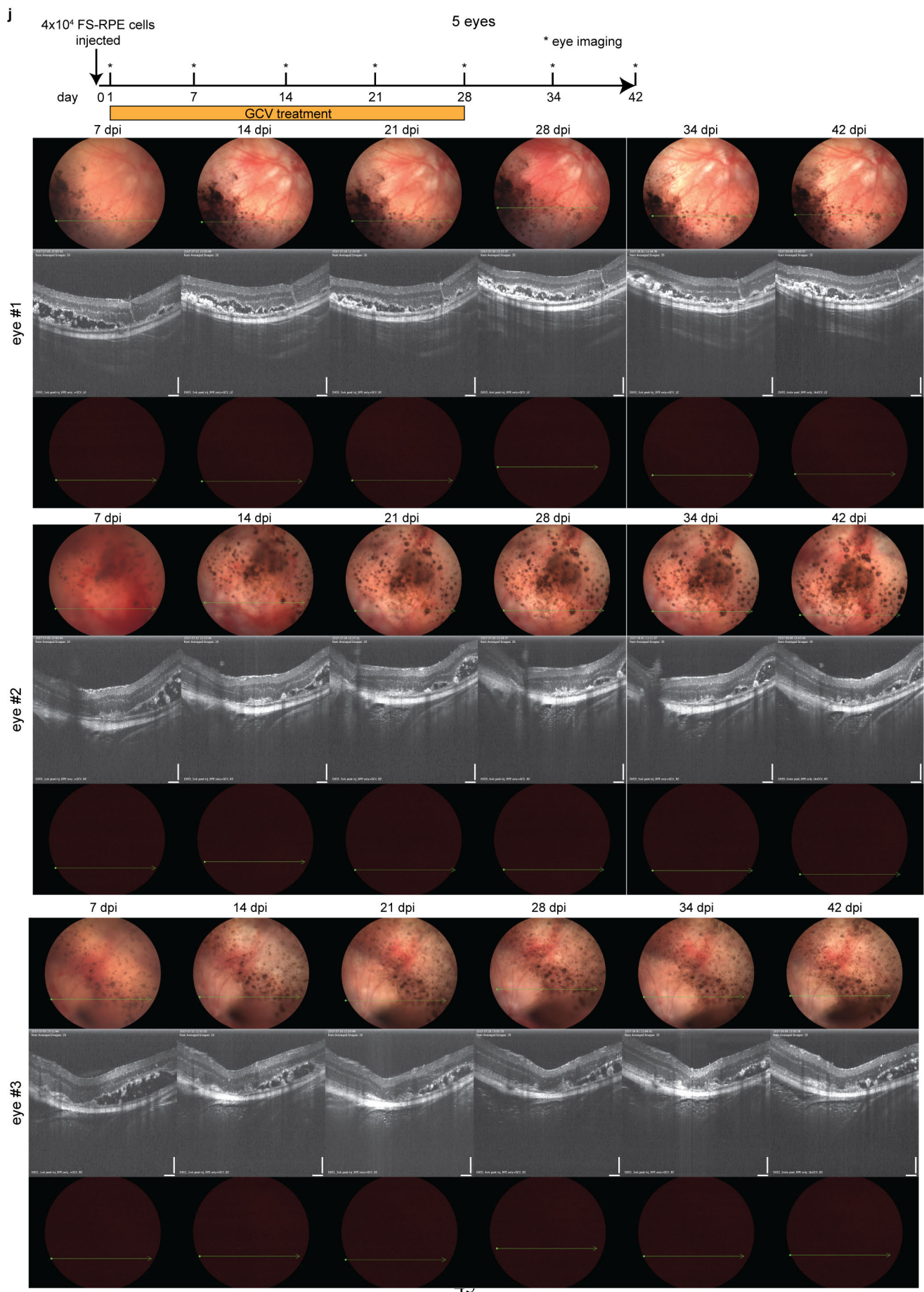
3x10<sup>4</sup> FS-RPE cells +  
1x10<sup>4</sup> FS-ES cells  
injected

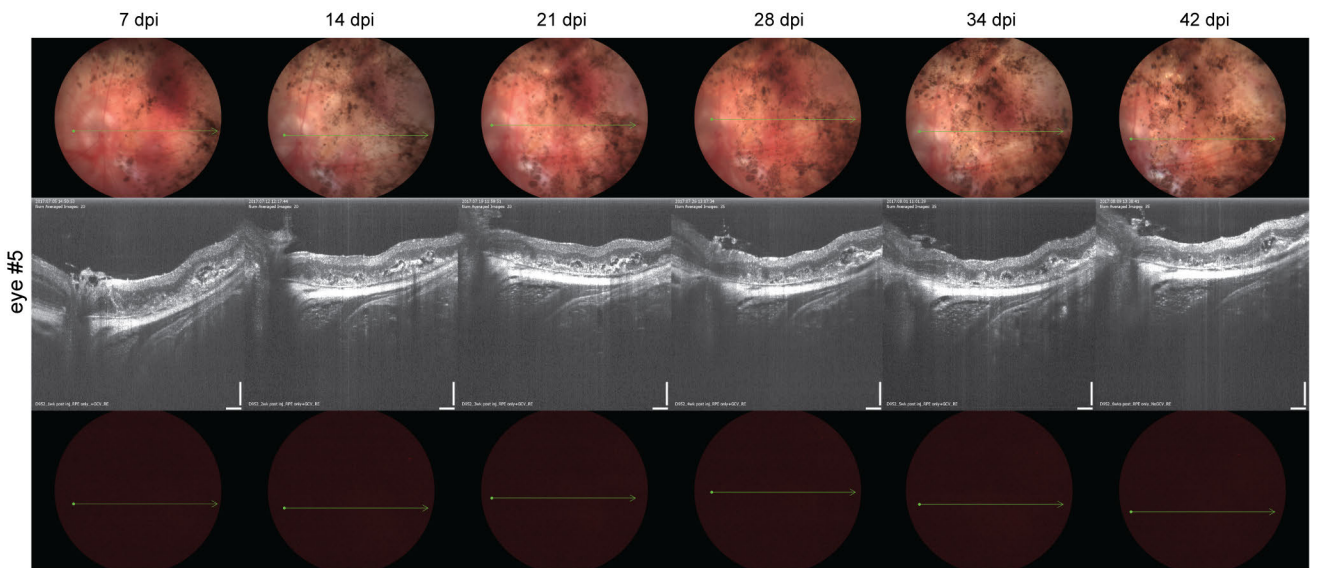
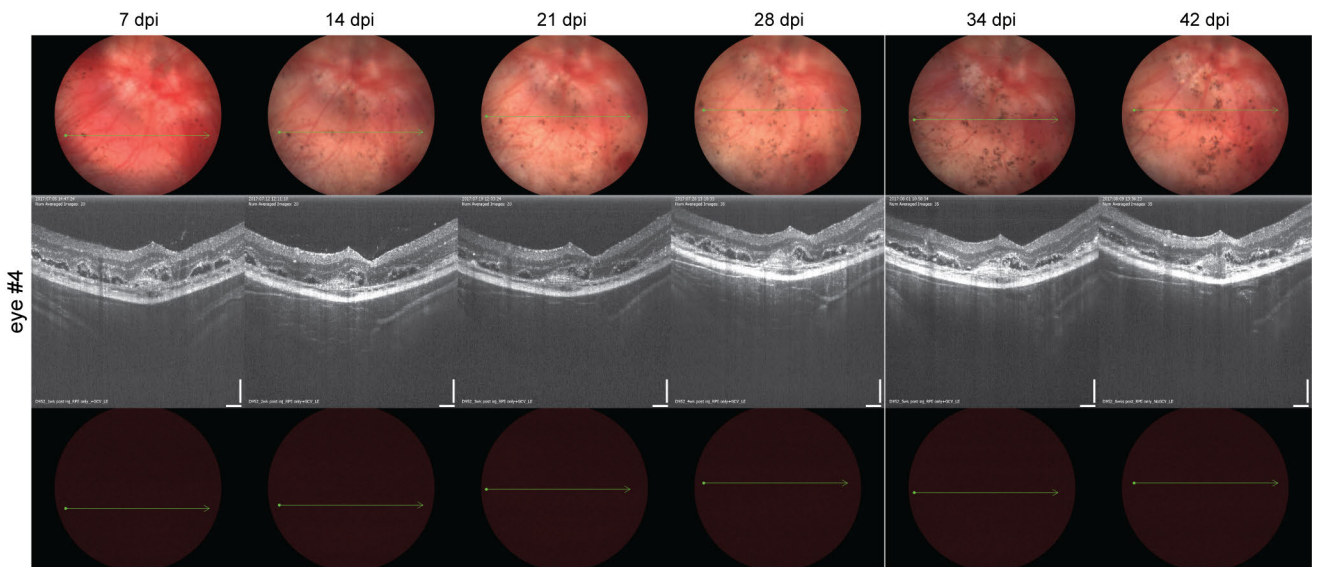


i

3x10<sup>4</sup> FS-RPE cells +  
1x10<sup>4</sup> FS-ES cells  
injected







821

k

4x10<sup>4</sup> FS-RPE cells injected

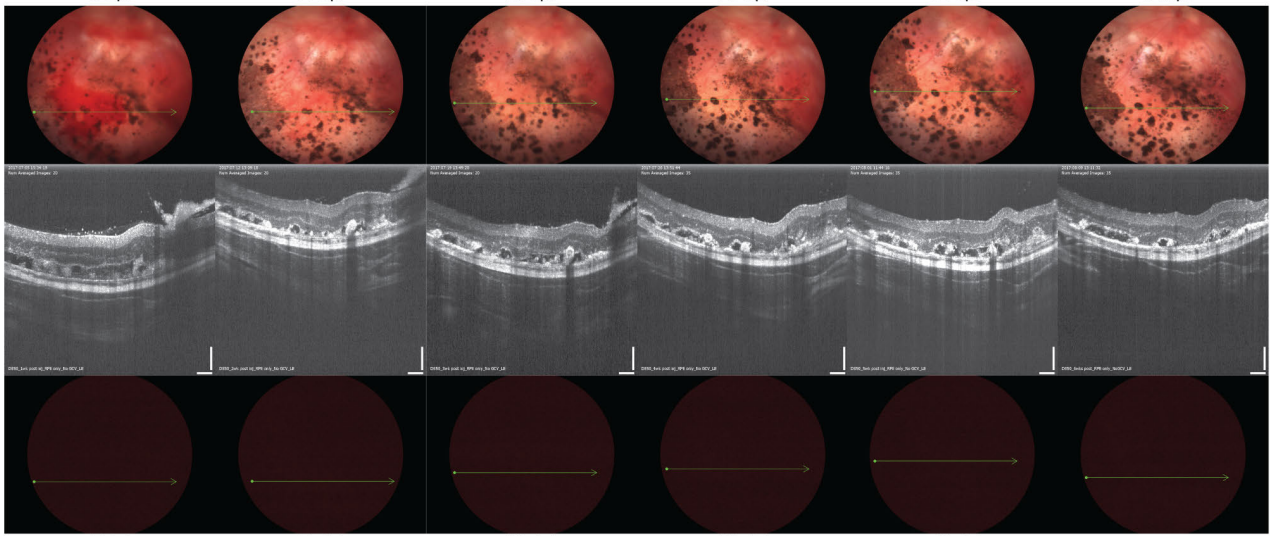
6 eyes

\* eye imaging

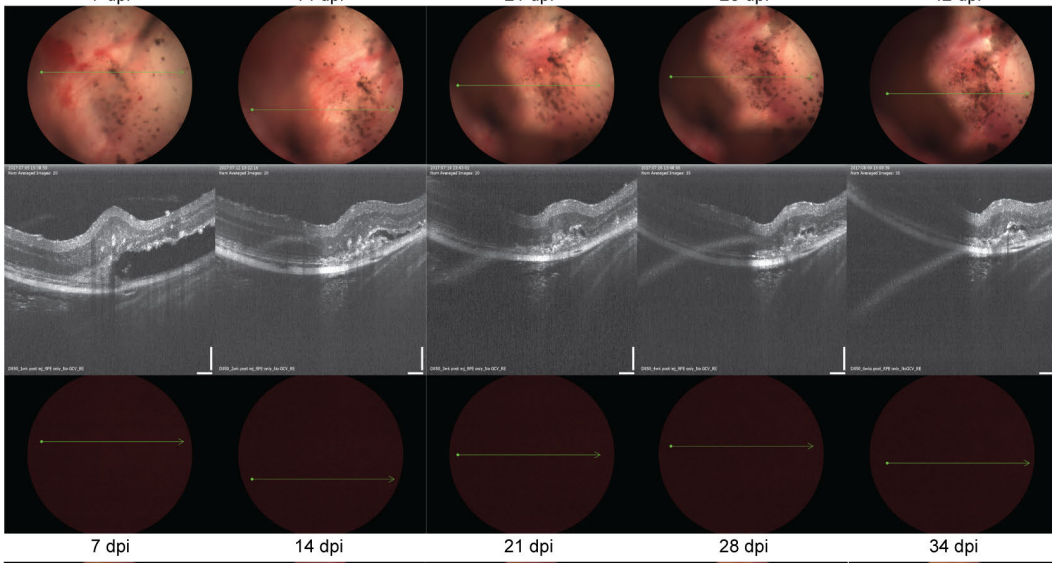
day 0 1 7 14 21 28 34 42

PBS treatment

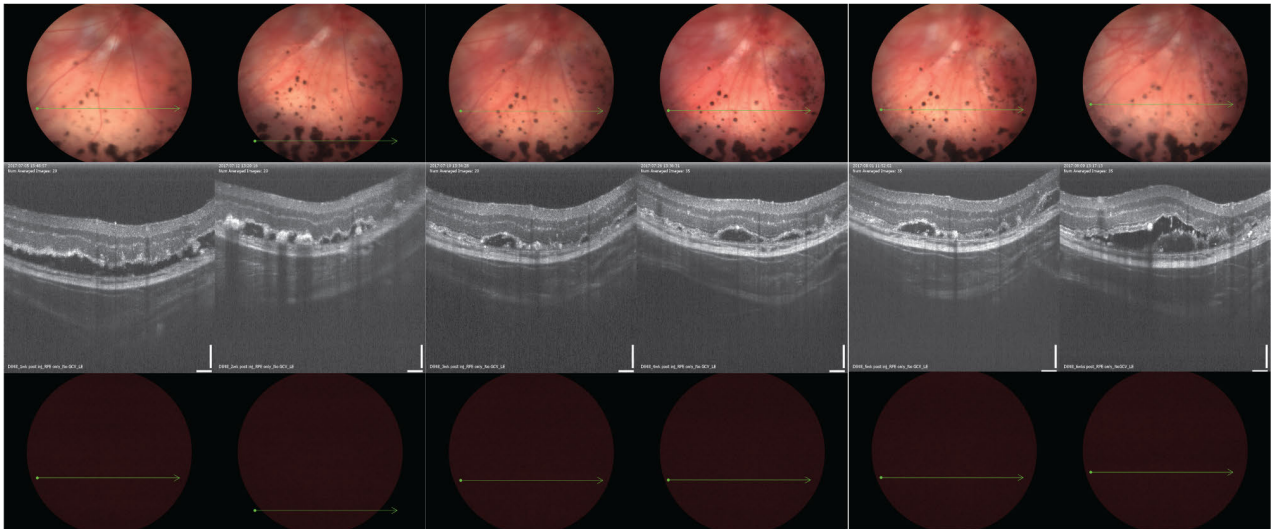
eye #1



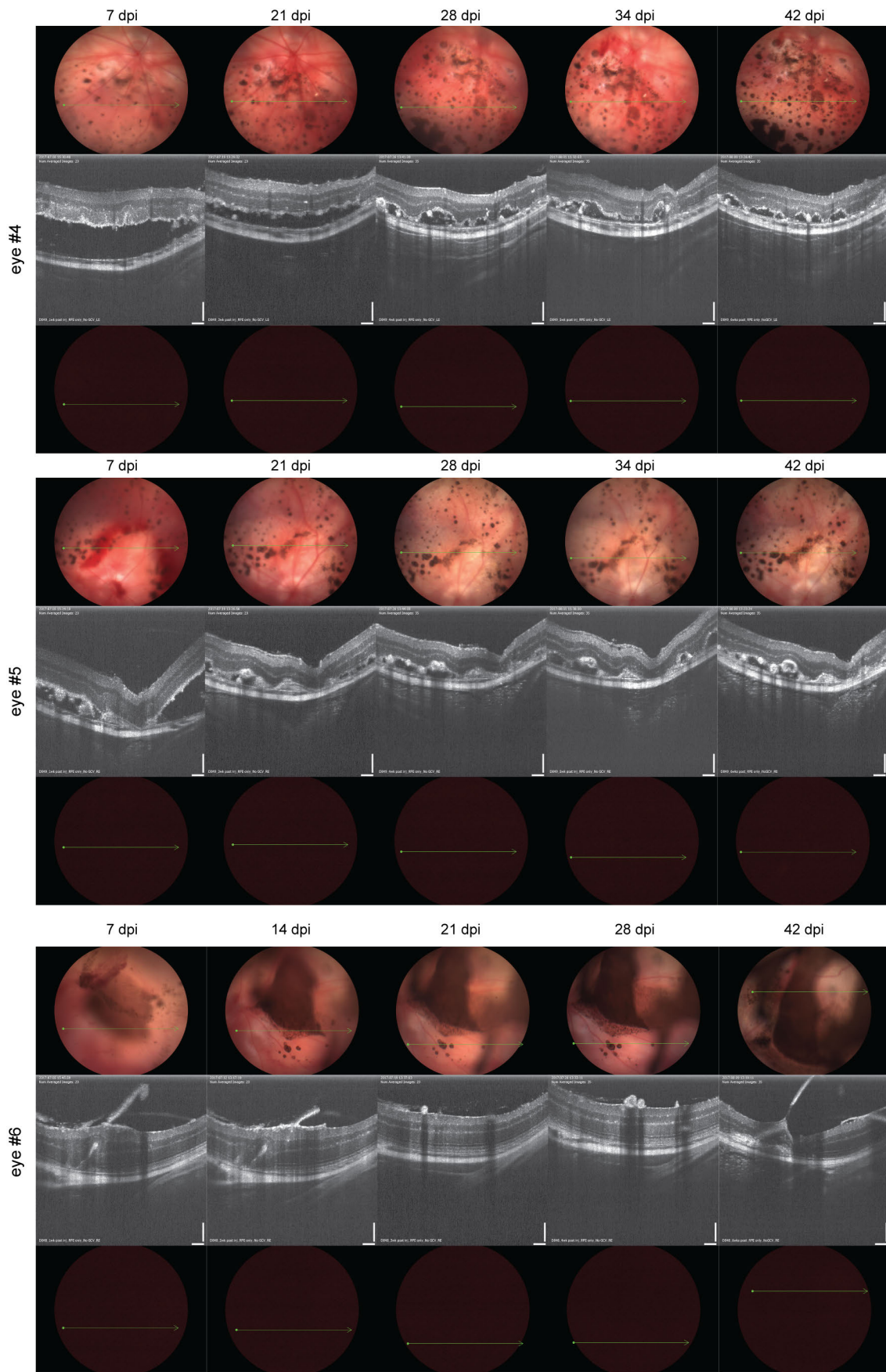
eye #2

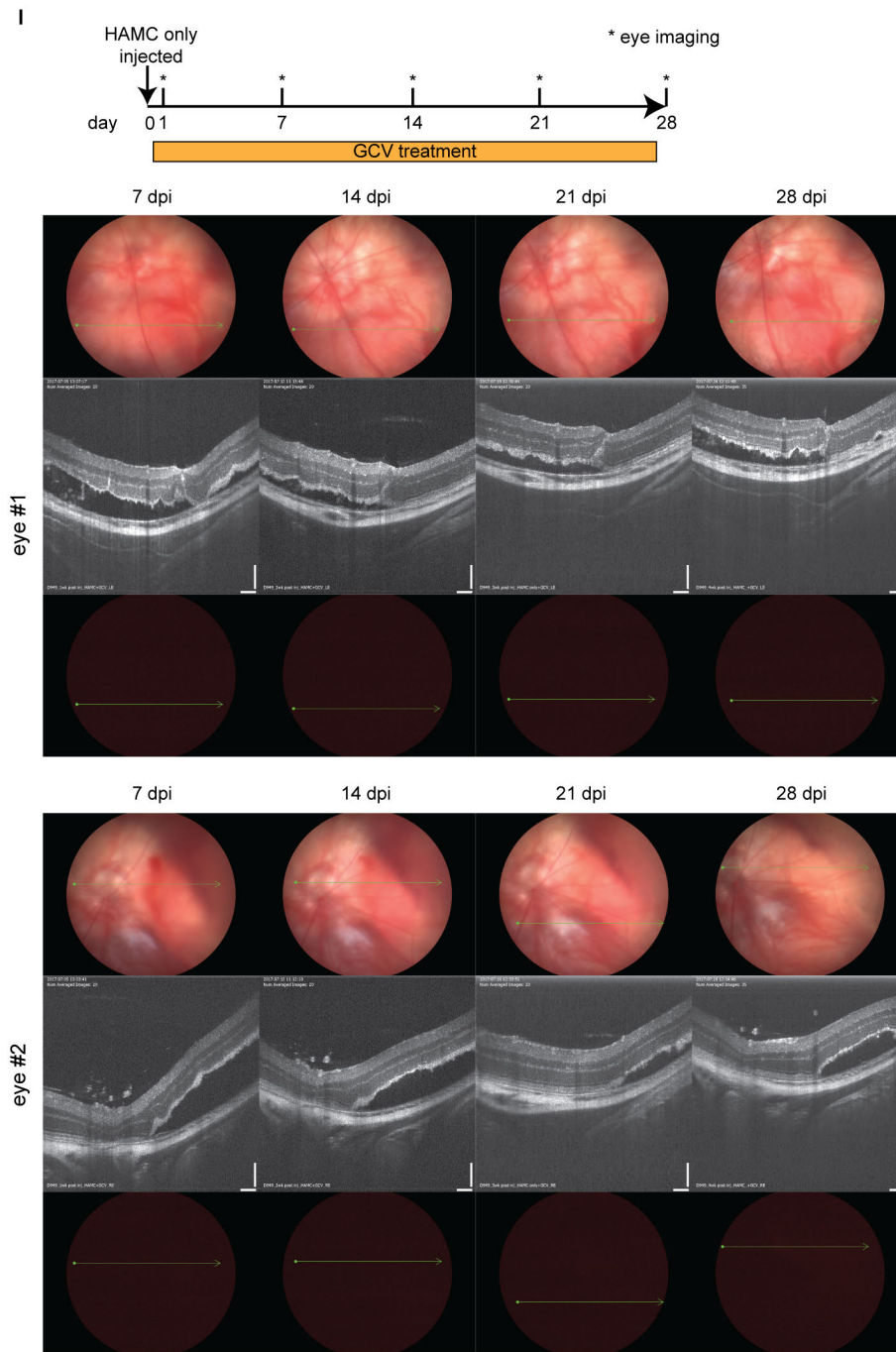


eye #3









824  
825

826 **Extended Data Figure 10 | Images of all eyes co-transplanted with FS-RPE and FS-ES cells (in**  
 827 **addition to Fig. 4), and images of all the eyes transplanted only with FS-RPE cells. a-c,**  
 828 Fundoscopy, OCT and fluorescence imaging of eyes co-transplanted with FS-RPE and FS-ES cells (4-  
 829 week GCV treatment). The absence of mCherry signal indicates that ES cell growth has not occurred.  
 830 The bottom panel in c includes the green fluorescence channel to illustrate that the observed signal in the  
 831 red fluorescence channel is actually autofluorescence. d, Histological analysis of the eye presented in e.  
 832 e-i, Fundoscopy, OCT and fluorescence imaging of eyes co-transplanted with FS-RPE and FS-ES cells  
 833 (PBS treatment). mCherry signal is detectable and indicates ES cell growth. GCV treatment began 3  
 834 weeks post-injection following an initial PBS treatment. j, Fundoscopy, OCT and fluorescence imaging  
 835 of eyes receiving only FS-RPE cells (4-week GCV treatment). This demonstrates that GCV treatment  
 836 did not affect the RPE cells. k, Fundoscopy, OCT and fluorescence imaging of eyes receiving only FS-

837 RPE cells (4-week PBS treatment). I, Fundoscopy, OCT and fluorescence imaging of eyes receiving  
838 only HAMC (4-week GCV treatment).

## Supplementary Calculation 1

### The Effect of Aliquoting on FSL Calculation

We consider a pool of  $N = 2^n$  cells that has  $FSL_p = 1/p$  for some  $p \in (0, 1)$ . This means  $p$  is the probability that the pool of cells is not FS. Below we calculate first the probability that a randomly selected cell aliquot of size  $M = 2^m$ ,  $m < n$  is FS, i.e., the probability that it contains only FS cells.

In our model the pool can have  $2^k$  non-FS cells with probability  $p_k$ , for  $k = 0, 1, \dots, n$ , such that  $p_{k+1} = p_k/2$  for  $k = 0, 1, 2, 3, \dots, n-1$ . Thus

$$p_k = p_{k-1}/2 = p_{k-2}/2^2 = \dots = p_0/2^k,$$

for  $k = 1, 2, \dots, n$ , and since  $1 - p$  is the probability that the pool is FS, we have

$$1 = 1 - p + \sum_{j=0}^n p_j = 1 - p + p_0(1 + 2^{-1} + \dots + 2^{-n}) = 1 - p + p_0(2 - 2^{-n}).$$

Hence

$$p_0 = \frac{p}{2 - 2^{-n}}, \quad p_k = p2^{-k}(2 - 2^{-n})^{-1}, \quad k = 0, 1, \dots, n.$$

Let  $q_a$  denote the probability that the aliquot is FS, and let  $q_{a|k}$  denote the conditional probability that the aliquot is FS given that the pool has  $2^k$  non-FS cells. Clearly, the conditional probability that the aliquot is FS, given that the pool is FS, is 1, and  $q_{a|k} = 0$  if  $N - 2^k < M$ , i.e., when  $k \geq n$ . Thus by the law of total probability

$$q_a = 1 - p + \sum_{k=0}^n p_k q_{a|k} = 1 - p + p \sum_{k=0}^{n-1} 2^{-k}(2 - 2^{-n})^{-1} q_{a|k}. \quad (1)$$

It remains to calculate  $q_{a|k}$ . To this end we imagine that we choose  $M$  cells randomly, consecutively and without replacement, from a pool of size  $N$  which has  $K := 2^k$  non-FS cells. The probabilities that the first chosen cell is FS, the second chosen cell is FS and that the  $j$ -th chosen cell is FS, are  $\frac{N-K}{N}$ ,  $\frac{N-K-1}{N-1}$  and  $\frac{N-K-j+1}{N-j+1}$ , respectively, for  $j < N - K$ . Hence

$$q_{a|k} = \frac{N-K}{N} \times \frac{N-K-1}{N-1} \times \dots \times \frac{N-K-M+1}{N-M+1} = \prod_{j=0}^{M-1} \frac{N-K-j}{N-j}. \quad (2)$$

Note that this value is the same as  $\binom{N-K}{M}$  divided by  $\binom{N}{M}$ , which is immediately understandable by viewing the selection as randomly choosing  $M$  cells out of  $N$ . The number of all, equally probable selections is  $\binom{N}{M}$ , and among them  $\binom{N-K}{M}$  are FS aliquots.

Now we calculate  $FSL_{ap}$ , the FSL of the randomly chosen aliquot. Using that  $FSL_{ap} = 1/(1 - q_a)$ ,  $FSL_p = 1/p$  and  $1 - p = (FSL_p - 1)/FSL_p$ , from equation (1) we get

$$FSL_{ap} = \frac{FSL_p}{1 - \sum_{k=0}^{n-1} 2^{-k}(2 - 2^{-n})^{-1} q_{a|k}}. \quad (3)$$

Notice that the contribution of the terms  $2^{-k}(2 - 2^{-n})^{-1} q_{a|k}$  in the summation of the above expression is negligible for large  $k$ . Therefore we get a good approximation for  $FSL_{ap}$  if we keep only the terms with  $k < m$ . In this case we can simplify expression (2) for  $q_{a|k}$  by

$$(N - K) \times (N - K - 1) \times \dots \times (N - M + 1)$$

to get

$$q_{a|k} = \frac{N-M}{N} \times \frac{N-M-1}{N-1} \times \frac{N-M-2}{N-2} \times \dots \times \frac{N-M-K+1}{N-K+1} = \prod_{j=0}^{K-1} \frac{N-M-j}{N-j}. \quad (4)$$

It is clear that

$$\frac{N-M-j}{N-j} < \frac{N-M}{N} = \frac{A-1}{A},$$

where  $A = N/M$  is the number of aliquots generated from the pool of cells. Thus for  $K := 2^k < M = 2^m$  we can approximate  $q_{a|k}$  from above by

$$\left(\frac{A-1}{A}\right)^{2^k},$$

and from (3) we get the approximation

$$FSL_{ap} \approx \frac{FSL_p}{1 - \sum_{k=0}^{m-1} 2^{-k-1} \left(\frac{A-1}{A}\right)^{2^k}}. \quad (5)$$

We note that this approximation is very good in practice for the range of  $M$  and  $N$  that we are using, when  $M$  is essentially smaller than  $N$ , which is more than a million.

Finally we calculate the ratio  $FSL_{ap}/FSL_a$ , called FSL drop, where  $FSL_a$  denotes the FSL of a separately produced pool with the same cell number  $M$  as that of the aliquot. By our observations, in the clinically relevant range, the logarithm of the FSL is approximately a linear function of the logarithm of the cell number of the pool, with slope close to minus one. This means, that in the clinically relevant range of cell numbers we have

$$\frac{FSL_p}{FSL_a} \approx \frac{M}{N} = \frac{1}{A}.$$

Consequently, from (5) we obtain

$$\frac{FSL_{ap}}{FSL_a} \approx \frac{1}{A(1 - \sum_{k=0}^{m-1} 2^{-k-1} \left(\frac{A-1}{A}\right)^{2^k})}. \quad (6)$$

The contribution of those terms of the sum in this formula, which correspond to large  $k$ , is very small. In other words, for large  $M$  only the first few terms (i.e. 15) of the sum should be considered, since the contribution of the other terms is negligible. This means, that practically the FSL drop depends only on the number of aliquots  $A$ , when the cell numbers of the aliquot and of the pool are sufficiently large. To make this argument more precise let  $d_m$  denote the right-hand side of (6) and estimate the error  $\varepsilon_l = d_l - d_m$  that we make when we sum the terms until  $l - 1 < m - 1$  in place of  $m - 1$  in (6). Clearly, for any  $l < m$  we have

$$\varepsilon_l = \frac{1}{A} \left( (1 - S_m)^{-1} - (1 - S_l)^{-1} \right) \leq \frac{S_m - S_l}{A(1 - S_m)^2} < \frac{t_l}{A(1 - S)^2}, \quad (7)$$

where for integers  $j \geq 0$  we use the notations

$$S_j := \sum_{k=0}^j 2^{-k-1} \left(\frac{A-1}{A}\right)^{2^k}, \quad S := \sum_{k=0}^{\infty} 2^{-k-1} \left(\frac{A-1}{A}\right)^{2^k}, \quad t_j := \sum_{k=j+1}^{\infty} 2^{-k-1} \left(\frac{A-1}{A}\right)^{2^k}.$$

Since  $f(x) = 2^{-x} r^{-2^x}$  is a decreasing function of  $x \in [0, \infty)$  for any  $r \geq 1$ , we get

$$t_l \leq \frac{1}{2} \int_l^{\infty} 2^{-x} r^{-2^x} dx = \frac{1}{2 \ln 2} \int_{2^l}^{\infty} y^{-2} r^{-y} dy \leq \frac{2^{-2l}}{2 \ln 2} \int_{2^l}^{\infty} r^{-y} dy = \frac{2^{-2l-1}}{\ln r \ln 2} r^{-2^l}, \quad (8)$$

with  $r := A/(A-1)$ . Notice that for every  $j \geq 0$

$$1 - S \geq 1 - \sum_{k=0}^j 2^{-k-1} - t_j = 2^{-j-1} - 2^{-2j-1} (\ln r \ln 2)^{-1} r^{-2^j} = 2^{-j-1} (1 - 2^{-j} (\ln r \ln 2)^{-1} r^{-2^j}).$$

Thus choosing the smallest integer  $j = j_0$  such that  $j_0 \geq 1 - \log_2(\ln r \ln 2)$ , we get

$$1 - S \geq 2^{-j_0-2} \geq 2^{-3} (\ln r \ln 2)$$

for all  $A \geq 2$ . Thus we have

$$(1 - S)^2 \geq 2^{-6} (\ln r \ln 2)^2.$$

Using this together with estimate (8), from (7) we obtain

$$\varepsilon_l < \frac{1}{A(\ln 2 \ln r)^3} 2^{-2l+6} r^{-2^l}$$

for all  $l \leq m$  and  $A \geq 2$ , where  $r = A/(A-1)$ . Hence by the simple estimate

$$\ln r = \ln(1 + (A-1)^{-1}) \geq \ln 2(A-1)^{-1},$$

valid for all  $A \geq 2$ , and since  $(\ln 2)^{-6} < 10$ , we get

$$\varepsilon_l < 10 \frac{(A-1)^3}{A} 2^{-2l+6} r^{-2^l} < 10A^2 2^{-2l+6} r^{-2^l}.$$

Thus we can see that even for relatively large  $A$ , say  $A = 512$ , the error is negligible if  $m > 15$  is replaced with 15 in the calculation of the FSL drop by the formula (6).